NAVAL POSTGRADUATE SCHOOL

MONTEREY, CALIFORNIA

THESIS

VISIBLE–NEAR INFRARED (VNIR) AND SHORTWAVE INFRARED (SWIR) SPECTRAL VARIABILITY OF URBAN MATERIALS

by

Kenneth G Fairbarn Jr

March 2013

Thesis Advisor: Fred A. Kruse
Second Reader: R.C. Olsen

Approved for public release; distribution is unlimited

THIS PAGE INTENTIONALLY LEFT BLANK

REPORT DOCUMENTATION PAGE			Form Approved OMB No. 0704–0188
Public reporting burden for this collection of information is estimated to average 1 hour per response, including the time for reviewing instruction, searching existing data sources, gathering and maintaining the data needed, and completing and reviewing the collection of information. Send comments regarding this burden estimate or any other aspect of this collection of information, including suggestions for reducing this burden, to Washington headquarters Services, Directorate for Information Operations and Reports, 1215 Jefferson Davis Highway, Suite 1204, Arlington, VA 22202–4302, and to the Office of Management and Budget, Paperwork Reduction Project (0704–0188) Washington DC 20503.			
1. AGENCY USE ONLY *(Leave blank)*	**2. REPORT DATE** March 2013	**3. REPORT TYPE AND DATES COVERED** Master's Thesis	
4. TITLE AND SUBTITLE VISIBLE–NEAR INFRARED (VNIR) AND SHORTWAVE INFRARED (SWIR) SPECTRAL VARIABILITY OF URBAN MATERIALS			**5. FUNDING NUMBERS**
6. AUTHOR(S) Kenneth G. Fairbarn Jr.			
7. PERFORMING ORGANIZATION NAME(S) AND ADDRESS(ES) Naval Postgraduate School Monterey, CA 93943–5000			**8. PERFORMING ORGANIZATION REPORT NUMBER**
9. SPONSORING /MONITORING AGENCY NAME(S) AND ADDRESS(ES) N/A			**10. SPONSORING/MONITORING AGENCY REPORT NUMBER**
11. SUPPLEMENTARY NOTES The views expressed in this thesis are those of the author and do not reflect the official policy or position of the Department of Defense or the U.S. Government. IRB Protocol number ___N/A____.			
12a. DISTRIBUTION / AVAILABILITY STATEMENT Approved for public release; distribution is unlimited			**12b. DISTRIBUTION CODE**

13. ABSTRACT (maximum 200 words)

The advent of relatively high spatial resolution hyperspectral imagery (HSI) provides a different perspective of the urban environment than lower spatial resolution hyperspectral data and either multispectral or panchromatic images. The objective of this thesis was to build and analyze a spectral library of urban materials and to understand how spectral variability affects the ability of classification algorithms to identify and discriminate various materials. The scope of the project was limited to non-vegetative impervious materials located on the Naval Postgraduate School campus. An airborne hyperspectral image, acquired September 30th 2011 was used for image-derived endmembers and a portable spectroradiometer was used to collect field spectra. Visual analysis of spectra was performed to assess intra- and inter-class variability and to identify spectral features and their causes. The spectral angle mapper (SAM) algorithm was used on the HSI data as a method to quantify intra-class spectral variability using a standard spectral angle. Classification maps were created with both SAM and mixture tuned matched filtering (MTMF) algorithms to determine how intra- and inter-class spectral variability affect the algorithm's ability to classify urban materials. The spatially complex nature of the urban environment negatively affected the performance of the SAM algorithm, but the ability to increase the spectral angle to account for materials with high spectral variability allowed improved inter-class discrimination. The MTMF algorithm was better suited for intra-class discrimination of materials.

14. SUBJECT TERMS Remote Sensing, Hyperspectral, Spectrometry			**15. NUMBER OF PAGES** 103
			16. PRICE CODE
17. SECURITY CLASSIFICATION OF REPORT Unclassified	**18. SECURITY CLASSIFICATION OF THIS PAGE** Unclassified	**19. SECURITY CLASSIFICATION OF ABSTRACT** Unclassified	**20. LIMITATION OF ABSTRACT** UU

NSN 7540–01–280–5500 Standard Form 298 (Rev. 2–89)
Prescribed by ANSI Std. 239–18

THIS PAGE INTENTIONALLY LEFT BLANK

Approved for public release; distribution is unlimited

VISIBLE–NEAR INFRARED (VNIR) AND SHORTWAVE INFRARED (SWIR) SPECTRAL VARIABILITY OF URBAN MATERIALS

Kenneth G. Fairbarn Jr.
Civilian, Department of the Navy
B.A., University of California, Santa Barbara

Submitted in partial fulfillment of the
requirements for the degree of

MASTER OF SCIENCE IN REMOTE SENSING INTELLIGENCE

from the

NAVAL POSTGRADUATE SCHOOL
March 2013

Author: Kenneth G. Fairbarn Jr.

Approved by: Dr. Fred A. Kruse
Thesis Advisor

Dr. R.C. Olsen
Second Reader

Dr. Dan Boger
Chair, Department of Information Sciences

THIS PAGE INTENTIONALLY LEFT BLANK

ABSTRACT

The advent of relatively high spatial resolution hyperspectral imagery (HSI) provides a different perspective of the urban environment than lower spatial resolution hyperspectral data and either multispectral or panchromatic images. The objective of this thesis was to build and analyze a spectral library of urban materials and to understand how spectral variability affects the ability of classification algorithms to identify and discriminate various materials. The scope of the project was limited to non-vegetative impervious materials located on the Naval Postgraduate School campus. An airborne hyperspectral image, acquired September 30, 2011, was used for image-derived endmembers and a portable spectroradiometer was used to collect field spectra. Visual analysis of spectra was performed to assess intra- and inter-class variability and to identify spectral features and their causes. The spectral angle mapper (SAM) algorithm was used on the HSI data as a method to quantify intra-class spectral variability using a standard spectral angle. Classification maps were created with both SAM and mixture tuned matched filtering (MTMF) algorithms to determine how intra- and inter-class spectral variability affect the algorithm's ability to classify urban materials. The spatially complex nature of the urban environment negatively affected the performance of the SAM algorithm, but the ability to increase the spectral angle to account for materials with high spectral variability allowed improved inter-class discrimination. The MTMF algorithm was better suited for intra-class discrimination of materials.

THIS PAGE INTENTIONALLY LEFT BLANK

TABLE OF CONTENTS

THIS PAGE INTENTIONALLY LEFT BLANK

LIST OF FIGURES

THIS PAGE INTENTIONALLY LEFT BLANK

LIST OF TABLES

THIS PAGE INTENTIONALLY LEFT BLANK

LIST OF ACRONYMS AND ABBREVIATIONS

AIS	Airborne Imaging Spectrometer
AVIRIS	Airborne Visible/Infrared Imaging Spectrometer
EMR	Electromagnetic Radiation
ENVI	ENvironment for Visualizing Images
FOV	Field of View
FWHM	Full Width Half Maximum
GSD	Ground Sample Distance
HSI	Hyperspectral Imaging
μm	Micrometers
MSI	Multispectral Imaging
MTMF	Mixture Tuned Matched Filtering
NDVI	Normalized Differential Vegetation Index
NIR	Near Infrared
nm	Nanometers
RGB	Red, Green, Blue
ROI	Region of Interest
SAM	Spectral Angle Mapper
SAMS	Spectral Analysis and Management System
SWIR	Short Wave Infrared
VIS	Visible
VNIR	Visible and Near Infrared
W	Watts

THIS PAGE INTENTIONALLY LEFT BLANK

ACKNOWLEDGMENTS

I would like to thank everyone who helped me get through this challenging year. Although I am typically too stubborn to ask for help when I need it the most, I was given a considerable amount of help and support by my family, friends, faculty, and staff. My scientific research and writing skills have improved significantly with the help of my thesis advisor, Dr. Fred Kruse. I would also like to thank Professor Olsen for accepting me into the Remote Sensing Intelligence program and working with me on building a curriculum that fit my needs.

THIS PAGE INTENTIONALLY LEFT BLANK

I. INTRODUCTION

This thesis explores the visible, near-infrared and short-wave-infrared (VNIR-SWIR) spectral variability of urban materials. Traditionally, urban mapping using remote sensing data has been accomplished using primarily geometric shapes that correspond to buildings, streets, and other features. A hyperspectral Image (HSI) acquired from an imaging spectrometer is comprised of a large number, typically hundreds, of narrow contiguous spectral bands spanning the visible (VIS) and solar-reflected infrared (Goetz, 2009). A better understanding of the spectral response of urban materials is needed to lay the ground work for spectral mapping of the urban environment using HSI data. Spectral mapping is the mapping of individual materials that a surface is composed of as opposed to more traditional urban mapping of features at a larger scale (i.e., entire buildings or city streets). Spectral identification and accurate mapping of these materials will provide new resources to city planners and allow them to accomplish tasks such as managing storm runoff by assessing the amount of impervious materials in a region, or identification of roofs made of flammable materials such as wooden shingles to assess fire risk. Another application would be to assess the age and wear of transportation surfaces using their spectral properties as a means to improve the management of transportation infrastructure (Herold, 2004). Applications that may be of interest to the department of defense could be the identification of materials used in explosive devices on transportation surfaces.

This thesis addresses the need to develop and utilize a spectral library specifically for the urban environment as well as the analysis of the spectral properties of the materials. Weathering, age, wear, and other factors affect the intra-class spectral variability of materials and because the urban environment is a constantly changing place with surfaces of all types, it is a perfect study area for this research. Although the data used for this study are of the Monterey, California, area, the techniques developed should be applicable to remote sensing of any urban material or area.

Previous work has been done regarding hyperspectral remote sensing of urban materials and areas; however, the focus of this research was to improve upon these results

by adding spectra of additional urban materials, better characterizing intra- and inter-class spectral variability, and improving analysis methods. Previous studies, such as (Herold, 2004), developed a spectral library of similar materials but this thesis addresses the need to expand the library to include a wider variety of intra-class spectra to capture the spectral variability that is intrinsic to urban materials. Spectral mapping of Airborne Visible/Infrared Imaging Spectrometer (AVIRIS) imagery is used to determine the performance of the spectral library in the mapping of known materials based on inter-class spectral variability.

II. BACKGROUND

A. GENERAL

1. History

Remote sensing was first developed to obtain a better perspective of urban areas by using balloons to photograph cities from a higher vantage point. These early attempts at urban remote sensing were great examples of applications of urban remote sensing, such as Gaspard-Felix Tourachon's 1868 photo of Paris from a balloon (Figure 1) (Olsen, 2007). Although the main purpose of this imagery may not have been strictly cartographic, it is now possible to analyze the image using some basic elements of recognition to determine where the streets, buildings, and other urban features are located. Aerial photography and the remote sensing platforms gradually improved through the early 20th century but panchromatic images were the standard until multispectral (MSI) and hyperspectral (HSI) imagery sensors were developed later in the 20th century.

Figure 1. Aerial photograph taken in 1868 by Gaspard-Felix Tournachon from the Hippodrome Balloon 1700 ft. above Paris. (From Olsen, 2007). Although the image has a relatively low spatial resolution, it is possible to recognize features such as streets and buildings.

Early remote sensing platforms and sensors were gradually improved with the use of reconnaissance airplanes during World War I, camera equipped V-2 missiles in 1946, film-return satellites in 1959, and the first color image of earth from lunar orbit in 1968. It was not until platforms such as Landsat 1 (formerly named Earth Resources Satellite 1) was launched in 1972 that wavelengths beyond the visible spectrum were utilized. These early systems were only capable of a general discrimination between various materials based on spectral features that fell within the wide spectral bands. Multispectral imagery and hyperspectral imagery that are now available can be used to identify specific minerals, species of plants, and other materials. Hyperspectral sensors are often used to select the optimal width and location within the electromagnetic spectrum to be used in a multispectral sensor. The systems utilized for this thesis use the Visible and near-infrared (VNIR) and shortwave infrared (SWIR) wavelengths to identify urban materials using a field spectroradiometer and airborne HSI.

2. Electromagnetic Radiation

Airborne and spaceborne sensors receive electromagnetic emissions in various spectral bands that reveal features on Earth and other phenomena (Sellers, 2005). Sensors from remote sensing systems can theoretically measure energy emanating from earth's surface in any practical wavelength range (Figure 2).

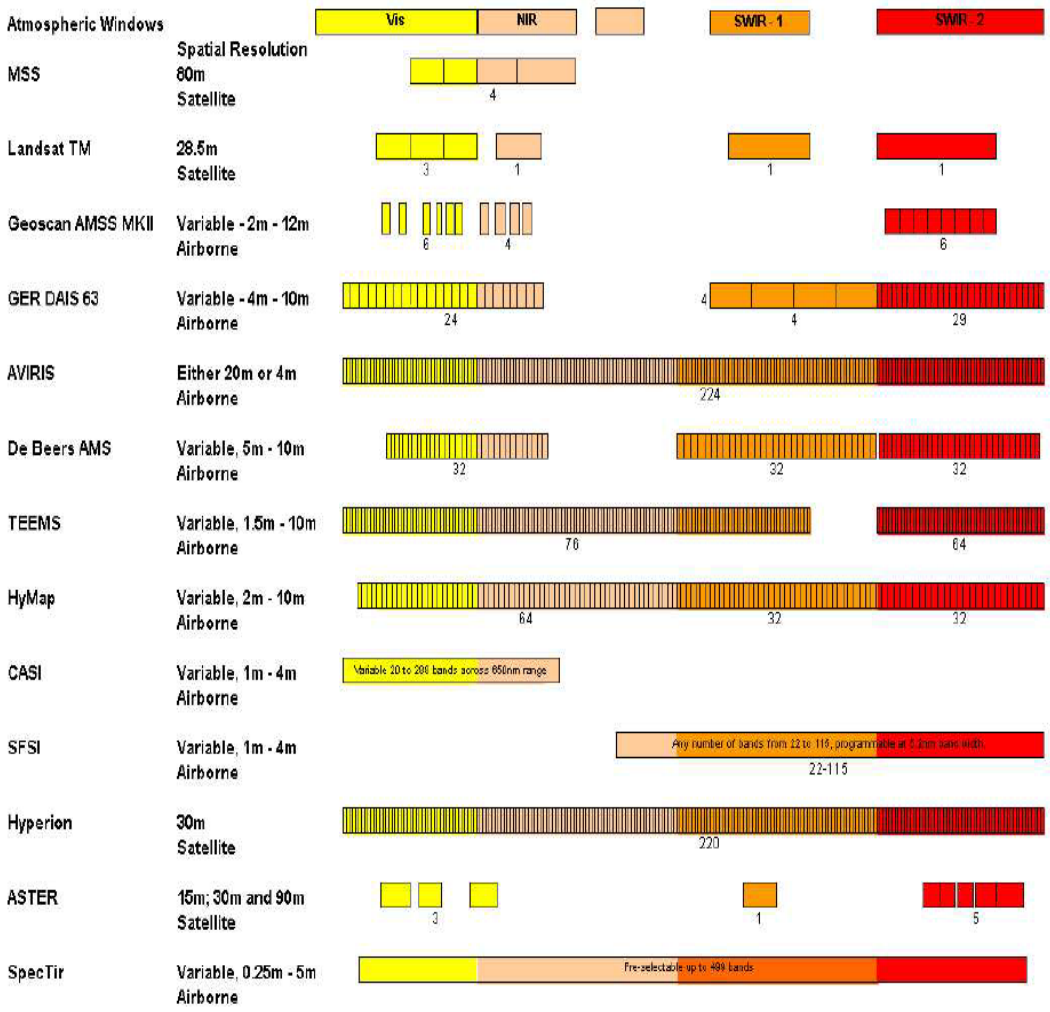

Figure 2. Comparison HSI and MSI spectral and spatial resolution. (From Agar & Coulter, 2007).

Some wavelengths, however, are more suitable than others for various remote sensing purposes. Remote sensing systems are designed with a spectral range and resolution that are suitable for a range of purposes based on the interaction mechanism between the electromagnetic radiation and the material being examined (Richards, 1999). Early remote sensing systems (as early as 1858), used panchromatic (black and white) film to view cities from a higher perspective. Because humans can only see in the visible range (400–700 nm) the first sensors only imaged in spectral ranges familiar to the human observer (Figure 3).

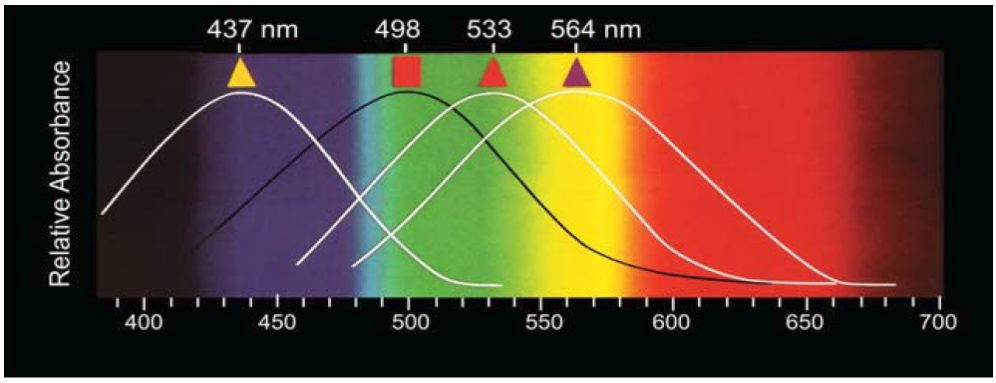

Figure 3. Visible spectrum is relative to the sensitivity of the human eye's rods (black curve) and cones (white curves) (From Olsen, 2007).

Elements of recognition such as shape, size, shadow, height, tone/color, texture, pattern, association, site and time are used to literally analyze this type of imagery (Olsen, 2007). Most modern hyperspectral sensors and some multispectral sensors utilize the full VNIR-SWIR spectrum. Hyperspectral Imagery and some multispectral imagery exploit bands in the wavelengths past 700 nm, near-infrared (NIR) ~700–1,000 nm and short wave infrared (SWIR) ~1,000–2,500 nm regions. Using these spectral bands, it is possible to perform non-literal analysis, measuring the reflected energy modified by surface physical properties such as pigmentation, moisture content and cellular structure of vegetation, the mineral and moisture content of soils and the level of sedimentation of water (Richards, 1999). The AVIRIS hyperspectral imagery and field spectrometers used in this thesis sample in the VNIR and SWIR wavelengths.

3. Radiance and Reflectance

Imagery used in this thesis was acquired using passive remote sensing systems that use the energy from the sun to illuminate Earth surface materials. Energy reflected from the surfaces is measured by the sensor either on a spaceborne or airborne platform. It is therefore important to understand the basic principles of radiance and how the atmosphere and surface materials interact with photons. The sun's energy propagates through space isotropically in an inverse square law fashion, so that at a given distance, the sun's emission can be measured as Watts per square meter (Richards, 1999). The radiation from the sun is referred to as insolation. Light interacts with matter in four

distinctive ways. Transmission is when there is no measurable attenuation of the incident radiation as it passes through matter. Reflection, or specular reflection, is when incident radiation bounces off matter in a single predictable direction. Scattering is when incident radiation is spread out unpredictably in many directions. Absorption is when incident radiation is taken in by the matter and converted to internal heat energy (Figure 4) (Olsen, 2007).

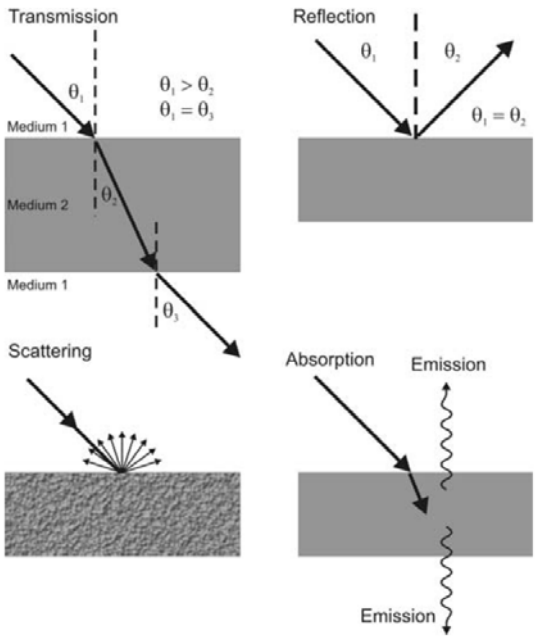

Figure 4. Transmission, reflection, scattering, and absorption of light when interacting with various surfaces (From Olsen, 2007).

The term hyperspectral imaging was first coined by Goetz, Soloman, & Rock (1985) as a reference to imaging spectrometry. Goetz et al. (1985) define imaging spectrometry as "the acquisition of images in hundreds of contiguous, registered, spectral bands such that for each pixel a radiance spectrum can be derived." The modifier "hyper" (meaning too much) in hyperspectral refers to the fact that most materials do not require hundreds of spectral bands to be identified Goetz (2009). Raw measurements of radiance are typically acquired as digital numbers (DN), which characterize the intensity of a pixel for a given wavelength. These are converted through sensor calibration

information to units of radiance, usually μW/cm^{2}nm/sr or equivalent. Because remote sensing systems do not directly measure reflectance, a further conversion of radiance into reflectance is needed to allow comparison to field and laboratory reflectance measurements. This is done by dividing the total radiance by the radiance of a near perfect reflector. For lab and field spectrometry applications, this is accomplished by collecting radiance from a material that is a near-perfect diffuse reflector throughout the entire spectral range that is being utilized (Figure 5).

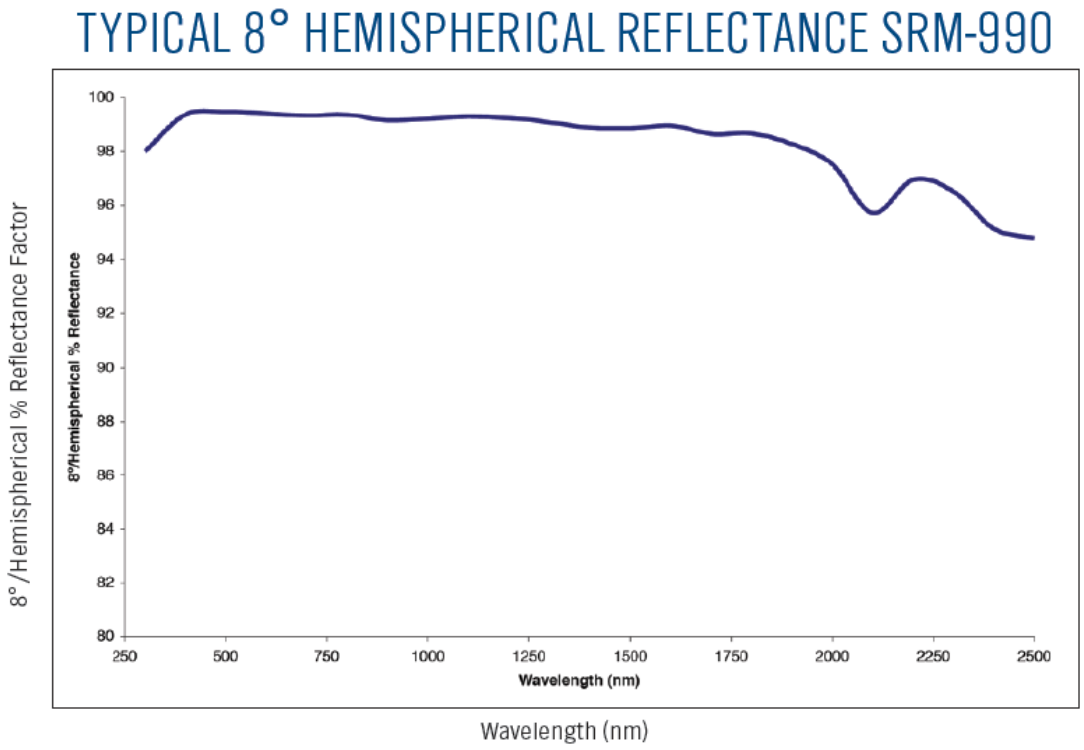

Figure 5. Percent reflectivity of a Spectralon target. Corrected reflectance values are above 92.5% across all wavelengths with 1650–2500 nm being the lowest (From Labsphere, 2012, www.labsphere.com).

Spectralon (www.labsphere.com) is the product most commonly used as a reference reflectance target and is made by the pressing halon (bromochlorodifluoromethane, CF_2ClBr) into a flat surface (Herold, 2004). The Analytical Spectral Devices (ASD) Fieldspec 4 spectroradiometer used in this thesis is able to either convert to reflectance

automatically or radiance values from the Spectralon panel can be saved and converted in post-processing. Roberts & Herold (2004) describe this process:

> Radiometric calibration is done by converting the DNs into spectral radiance, L_λ, through a series of wavelength dependent instrumental gains and offsets (L_λ=Gainλ*DNλ+offsetλ). Instrumental gains and offsets are typically established in the laboratory using a calibrated light source and integrating sphere (prelaunch gains and offsets). Instrumental performance, however, can also be monitored in flight using on-board light sources and the instrumental gains and offsets can be adjusted after a flight has occurred using ground targets. (Roberts & Herold, 2004)

For the purposes of spectral identification of materials, reference spectra of well characterized materials need to be measured. These are typically measured under controlled conditions for known materials and compiled into a spectral library. A spectral library is a collection of spectral curves collected either in the field or laboratory with a spectroradiometer, or pure pixels (endmember spectra) can be derived from hyperspectral images. There are many spectral libraries publicly available. Comprehensive spectral libraries of minerals and vegetation are made available by the United State Geological Society (USGS) and the Jet Propulsion Lab (Clark 1993; Grove 1992). Roberts and Herold (2004) developed an urban spectral library of the Santa Barbara area. Specialized libraries, such as those for urban materials, are less common, so it is typically necessary to compile specific spectral libraries for the study areas of interest to allow accurate identification of these materials (McCoy, 2005). The existing spectral libraries are of mostly pure minerals such as quartz or kaolinite, where specialized spectral libraries (i.e., urban libraries) are typically composed of a variety of materials that intrinsically have relatively high inter-class spectral variability. The spectral library developed for this thesis tries to capture the variability within classes of materials (intra-class variability) by compiling a library of several variations of a single material.

The spatial component of field spectroradiometers is much simpler than hyperspectral imagers because hyperspectral imagers actually create images with a spectrum at each pixel, while spectroradiometers just record the spectra of a field of view (FOV). The spectroradiometer foreoptic (lens) is typically between 1 degree and 25 degrees when using natural lighting (or artificially lit in lab) but a bare fiber optic (no

lens) can also be used with an internally lit foreoptic called a contact probe. The contact probe is the most precise and consistent method for collecting spectra because most of the lighting and imaging geometry are controlled. Therefore, spectra will vary much less given any lighting condition or location. Deriving endmembers (pure pixels with minimal spectral mixing) from hyperspectral images can also be used to create a spectral library. This is quick and efficient, but there are many assumptions about the hyperspectral geometric and environmental conditions that are made that may affect resulting spectra.

McCoy (2005) describes the many factors, or assumptions, that affect the reflectance spectra when using hyperspectral imagers or spectroradiometers. Assumption one is that the field of view, (FOV), of the sensor is known (Figure 6). This field of view is described as the tangent of (θ), one-half the angle of the instrument's field of view, multiplied by the distance (d), gives the radius (r) of the field of view at the target.

$$r = d \tan \theta \quad (1)$$

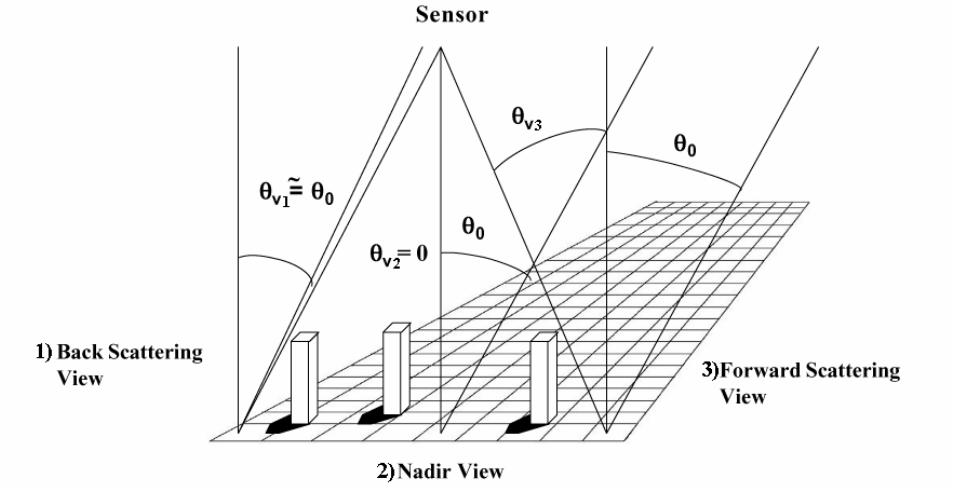

Figure 6. Illumination geometry of an imaging spectrometer given a scene with buildings (From Roberts & Herold, 2004).

The FOV will be known when collecting endmembers from hyperspectral images, but the spatial extent of the pixels used will depend on the accuracy of the ground-truth data and the heterogeneity of the surface being sampled. Assumption two (only relevant

to field spectroradiometers) is that the FOV will fill the standard reference panel. This is important because the reference panel is used to collect a white reference and any adjacent material will affect the measurement. Assumption three is that the target fills the FOV. When working with small targets, the peripheral area may be included in the FOV. Assumption four is that irradiance is constant while measuring both the reference panel and the target. This is difficult if clear skies are not typical where you are collecting. Assumption five is that the direct solar irradiance is the dominant source of energy incident on the target. Even on a clear day, up to 90% of the total energy incident on target is from solar irradiance and on hazy days the proportion of scattered skylight increases. Assumption six is that the sensor has a linear response to changes in radiation. This is dependent on the manufacturer of the spectroradiometer but needs to be considered. Assumption seven states that the reflectance of the standard panel at various wavelengths is known and they do not change during the course of work. The need to use the reflectance panel in the field subjects it to dirt, moisture, and contaminants that may alter the panel and affect the integrity of the measurements (McCoy, 2005)

4. Hyperspectral Imaging or HSI (Imaging Spectrometry)

The theory behind hyperspectral remote sensing is that the reflected solar radiation from Earth surfaces can be measured in hundreds of spectral images across a contiguous wavelength region. These spectral images are referred to as bands, and when stacked, they are referred to as the spectral cube (Figure 7). Most imaging spectrometers and field spectroradiometers acquire data in 10 nm wide bands, which is sufficient to capture spectral features that are between 20–40 nm in width at the half-band depth, the "full-width-half-max or FWHM" (Vane, 1988).

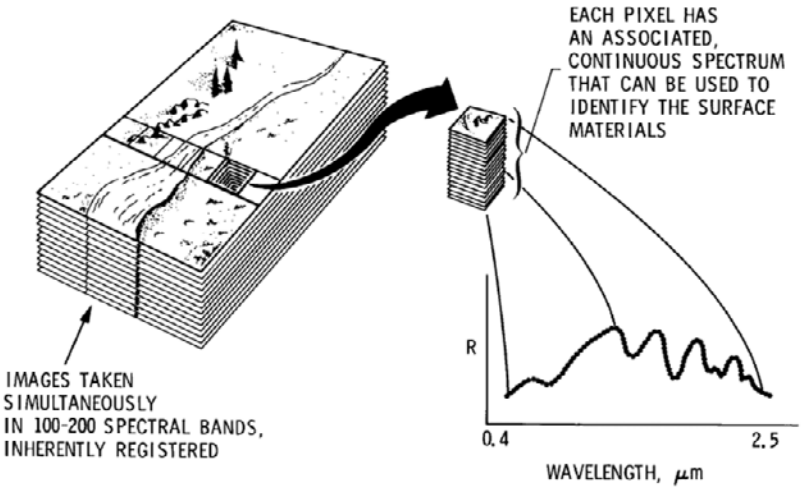

Figure 7. Diagram of the imaging spectroscopy concept and how a continuous spectrum can be a unique identifier to a particular pixel (From Goetz, 1988).

This thesis involves analysis of airborne hyperspectral imagery as well as field spectroradiometer data, therefore it is important to understand and review how and why this technology was developed. Prior to HSI, multispectral imagery were available from systems such as the Landsat Thematic Mapper. Landsat was revolutionary for its time because it utilized wavelengths beyond the visible spectral range (400–700 nm). It only had 6 spectral bands in the VNIR-SWIR, however, lacking the hundreds of contiguous spectral bands that allow imaging spectrometers to not only discriminate between surfaces but to actually identify rocks, soils, vegetation, water, and ice based on their reflectance and emittance spectra.

Although spectrometry was used extensively prior to earth remote sensing applications in planetary science as well as other fields, airborne and spaceborne

spectrometry got its start with the Shuttle Multispectral Infrared Radiometer (SMIRR), which led to the development of the Airborne Imaging Spectrometer (AIS) and finally the modern hyperspectral imagers, including the current state-of-the-art Airborne Visible/Infrared Spectrometer (AVIRIS) used for this thesis. In 1981, the Shuttle Multispectral Infrared Radiometer (SMIRR) was used to prove that minerals could be identified from earth orbit using a spectrometer (Goetz, 2009). SMIRR had 10 non-contiguous bands throughout the VNIR and SWIR and was able to use the 5 bands in the 2200 to 2500 nm region to successfully identify limestone and the mineral kaolinite (Goetz, 1987). SMIRR was not a true imaging spectrometer, but rather an orbiting spectroradiometer, because it collected only one point or pixel that was georeferenced using a panchromatic camera that was aligned with SMIRR. AIS-1 was introduced in 1982 for mineral mapping and is considered the first airborne hyperspectral imaging system (Goetz et al., 1985). This was a "fundamentally new class of data," which required researchers to develop new ways to extract information (Vane, 1988). AIS-1 had a spectral range of 900–2100 nm (tree mode) and 1200–2400 nm (rock mode) with 9.3 nm bandwidth (Goetz et al., 1985). The shortcomings of AIS were mainly the narrow field-of-view, low signal-to-noise ratio (SNR), and inadequate radiometric calibration. Although there were several imaging spectrometers being developed in the 1980s, AVIRIS became the primary imaging spectrometer for earth remote sensing because of its high SNR and radiometric fidelity. AVIRIS improved upon AIS by including full spectral coverage from 400–2450 nm with 224 spectral bands. One of the major improvements was that AVIRIS was radiometrically calibrated; therefore allowing researchers to obtain apparent surface reflectance through the use of atmospheric models. Analysis of AIS typically relied on using data-based methods such as taking the running average of the data then dividing the spectra by the mean to get to relative reflectance. Because AVIRIS is radiometrically well-characterized, the use of atmospheric models for correction to reflectance is possible and thus spectral features are more apparent and quantitative analysis is possible. Other airborne and spaceborne spectrometers are available now that cover spectral ranges similar to AVIRIS, but these vary in spatial, spectral, and temporal resolution. Notably, Hyperion is the spaceborne equivalent to

AVIRIS for spectral range, but has lower spatial resolution and higher temporal resolution. Its performance, however, is somewhat hampered by low SNR (Kruse, Boardman, Huntington, Mason, Quigley, 2002). Other historical and available hyperspectral imagers are listed in Table 1 for comparison. This thesis utilized AVIRIS because of its high radiometric performance and the relatively high spatial resolution needed for remote sensing of urban areas. The need for high spatial resolution will be discussed later.

Sensor	Spectral Range	FWHM	FOV	IFOV	GIFOV	Quantization
AVIRIS	370-2500 nm	10nm(nom)	32 deg	1mr	(20m/20km)	12 bit
	(224 bands)	(9.8nm samp)			(4m/4km)	
CASI	400-1000nm	2.2nm	37.8deg	1.25mr	(0.5m/0.4km)	12 bit
	(19 to 288 bands)	(1.9m samp)			(10m/8km)	
DAIS7915	450-2450nm	400-1000nm	51.2deg	3.3mr	(5m/1.5km)	15 bit
	(72 bands)	(15-30 nm, 32)			(20m/6km)	
	7 thermal	1500-1800nm				
		(45nm, 8)				
		2000-2500nm				
		(20nm, 32)				
HYDICE	400-2500nm	10nm (nom)	8.9 deg	0.5mr	(1m/2km)	12bit
	(210 bands)				(4m/8km)	
HyMAP	450-2500nm	15-22 nm	30-65deg	1-3mr	(1.5m/1.5km)	12-16bit
	(126 bands)	(VNIR 15-17nm)			(13.5m/4.5km)	
		(SWIR 17-22nm)				
MIVIS	430-830nm	20 nm	71 deg	2 mr	(5m/2.5km)	12 bit
	(20 bands)					
	1150-1550 nm	50 nm				
	(8 bands)					
	1985-2479 nm	8 nm				
	(64 bands)					
	10 thermal					

Table 1. Selected airborne imaging spectrometers suitable for urban remote sensing and their key attributes (From Herold, 2004).

With this fundamentally new class of data, image processing and analysis methods for imaging spectrometer data needed to be developed to handle the high dimensionality and the volume of data. Previous analysis of imagery was more qualitative but now hardware and software were needed to quantify and analyze each individual spectral image. Specialized software was developed to take advantage of the analysis of these features. One of these, "the Environment for Visualizing Images" (ENVI) was the primary software used for this thesis.

5. Spectral/Spatial Resolution Requirements and Considerations

The spatial requirements of hyperspectral imagery are mainly dependent on the homogeneity and size of the features being studied in the image. For homogenous areas such as sand dunes, large pixel sizes will not change the result as much as urban areas where spectral mixing can occur in even the highest resolution hyperspectral images. Multispectral and panchromatic images typically have a relatively high spatial resolution and are defined by a low spectral resolution. Hyperspectral imagery are typically of lower spatial resolution and defined by a higher spectral resolution. The advantage of hyperspectral data is the ability to identify materials rather than just discriminate between various materials.

Roberts & Herold (2004) define spectral resolution as the minimum spectral separation required to discriminate two spectral features. A spectral feature (i.e., spectral absorption) will only be visible if it falls within the FWHM as seen in Figure 8. Typically, multispectral sensors are designed for specific applications and place the band centers and band spacing to capture a particular feature. AVIRIS has a FWHM of 10 nm and spectral calibration of 0.5 nm or greater (Roberts & Herold 2004).

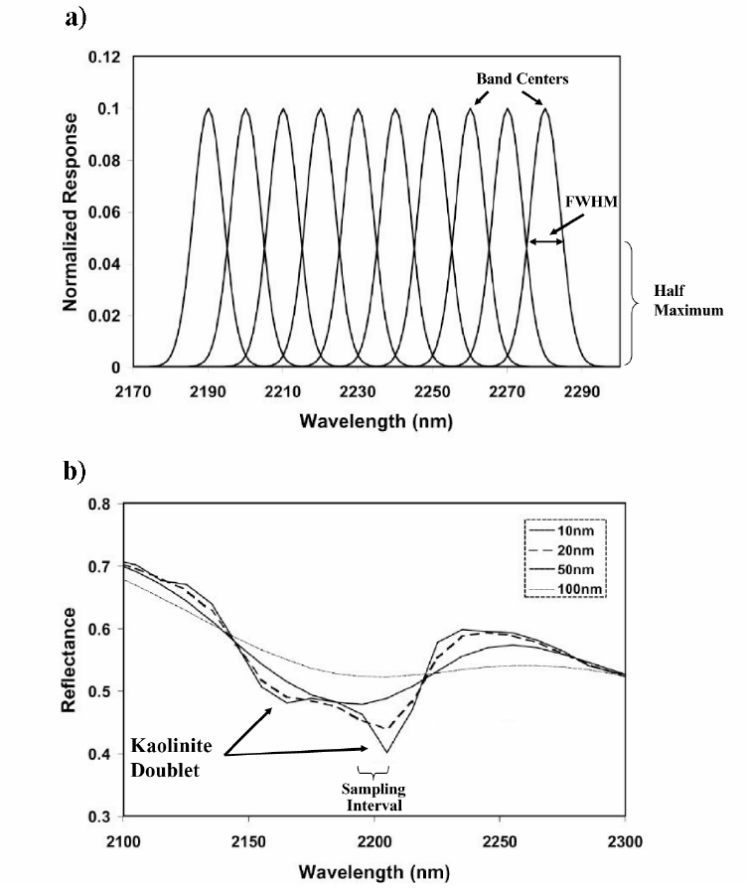

Figure 8. (a) The top plot shows the bands centers and shows how the FWHM is measured. (b) The bottom plot shows how the two unique spectral features in kaolinite are identifiable with a FWHM of 10 nm and not with a FWHM greater than 10 nm (From Roberts & Herold 2004).

It is rare to have a "pure" pixel, (one pixel with just one material and thus one spectral signature) in remote sensing data. Instead, most pixels have several materials and the resulting spectral signature is a mixture of the individual spectra (Figure 9). Spectral unmixing is the process of unmixing endmembers from a single pixel. An endmember spectrum represents a pure material with little or no mixing. An approach called the Pixel Purity Index (PPI) is often used to select the most spectrally pure (extreme) pixels, which are typically used as endmembers (Boardman & Kruse, 2011). This is an important aspect of hyperspectral image analysis for mineral mapping, and also urban applications, because hyperspectral imagery will often have low spatial resolution and a pixel will cover more than one urban feature.

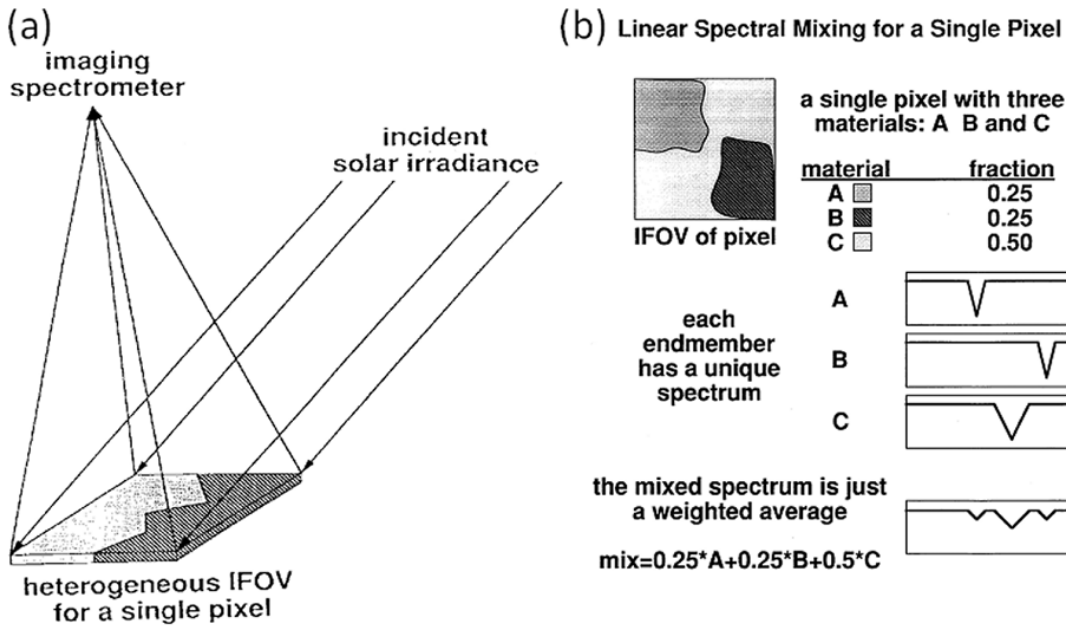

Figure 9. (a) The figure on the left shows the physical model for spectral mixing. (b) The figure on the right shows plots illustrating the three materials that are represented in the FOV of one pixel and how the spectral features of each material are weighted in the mixed spectrum of the single pixel (From Boardman and Kruse, 2011).

Spectral unmixing allows components of a pixel to be quantified. Richards (1999) describes the process mathematically. Assume *M* pure cover types, endmembers, in the image. The proportions of the endmembers the mixed pixel are represented by

$$f_m, m = 1,...M \tag{2}$$

Let $R_n, n = 1,...N$ be the observed reflectance of the pixel in the *nth* band of the *mth* endmember. ξ_n is the error is band *n* which is the extent that the observed reflectance in each band is the linear sum of the reflectance's of the endmembers Richards (1999).

$$R_n = \sum_{m=1}^{M} f_m a_{n,m} + \xi_n \;\; R_n = \sum_{m=1}^{M} f_m a_{n,m} + \xi_n \quad n=1,\ldots\mathrm{N} \tag{3}$$

Urban areas are a special case when considering spectral and spatial resolution. The diversity of materials in the urban environment such as various roofing materials, concrete, asphalt, soils of various ages and compositions, along with the three-

dimensional surface heterogeneity make it a very challenging environment to map (Herold 2003). Price (1997) found that only six bands from various AVIRIS hyperspectral imagery, mostly natural with some urban, described 99% of the spectral variability. Given the highly variable range of surfaces in urban areas, it is necessary to use more bands than in natural areas. urban remote sensing

6. Classification of Urban Materials

Classification of hyperspectral data using a spectral library approach is a complicated task for the urban environment because of the variety of materials found. Because, the urban environment is commonly composed of materials that occur in a variety of other settings, however, analysis methods can be adopted from other areas of research such as geologic mapping. There is a certain degree of land cover heterogeneity and there are several classification methods that capture that aspect, but a classification method designed specifically for urban remote sensing data is preferred due to the focus on scale. Anderson, Hardy, Roach, and Witmer (1976) include much more categories that are not necessarily needed for urban remote sensing; therefore, the Herold (2004) classification scheme is more practical for this application. The levels are representative of the scale of land cover. Anderson et al. (1976) use a sensor specific scale as seen in Table 2. Herold (2004) use a classification method that was aggregated from the Anderson et al. (1976) land cover classification specifically designed for remote sensing data (Table 3).

Classification Level	Typical data characteristics
I	LANDSAT (formerly ERTS) type of data
II	High-altitude data at 40,000 ft (12,400 m) or above (less than l:8O,OOO scale)
III	Medium-altitude data taken between 10,000 and 40,000 ft (3,100 and 12,400 m) (1:20,000 to 1:80,000 scale)
IV	Low-altitude data taken below 10,000 ft (3,100 m) (more than 1:20,000 scale)

Table 2. Classification levels Anderson et al. (1976) created for various scales of remote sensing data.

Level 1	Level 2	Level 3	Level 4
1. Built up	1.1 Buildings/roofs	1.1.1 Composite shingle roof	1.1.1.1 Black shingle
			1.1.1.2 Blue shingle
			1.1.1.3 Brown shingle
			1.1.1.4 Green shingle
			1.1.1.5 Grey shingle
			1.1.1.6 Mixed shingle
			1.1.1.7 Orange shingle
			1.1.1.8 Red shingle
			1.1.1.9 Tan shingle
			1.1.1.10 White shingle
		1.1.2 Plastic roofs	
		1.1.3 Glass	1.1.3.1 Light Glass
		1.1.4 Gravel roof	1.1.4.1 Gray gravel
			1.1.4.2 Red gravel
		1.1.5 Metal roof	1.1.5.1 Brown metal
			1.1.5.2 Light grey metal
			1.1.5.3 Green metal
		1.1.6 Asphalt roof	1.1.6.1 Light grey asphalt
		1.1.7 Tile roof	1.1.7.1 Red tile
			1.1.7.2 Gray tile
		1.1.8 Tar roof	1.1.8.1 Black tar
			1.1.8.2 Brown tar
		1.1.9 Wood shingle roof	1.1.9.1 Dark wood shingle
	1.2 Transportation areas	1.2.1 Asphalt roads	1.2.1.1 Light asphalt (old)
			1.2.1.2 Dark asphalt (new)
		1.2.2 Concrete roads	1.2.2.1 Light concrete
		1.2.3 Gravel roads	1.2.3.1 Light Gravel
		1.2.4 Parking lots	1.2.4.1 Dak Parking lot
		1.2.5 Railroad	1.2.5.1 Railroad tracks
		1.2.6 Walkways	1.2.6.1 Light concrete
			1.2.6.1 Red brick
		1.2.7 Street paint	1.2.7.1 White street marks
			1.2.7.2 Yellow street marks
			1.2.7.3 Red street marks
			1.2.7.4 Blue street marks
			1.2.7.5 Other street marks
	1.3 Sport infrastructure	1.3.1 Tennis courts	
		1.3.2 Red Tartan	
		1.3.3 Basketball court	
2. Vegetation	2.1 Green vegetation		
	2.2 Non-photosynthetic vegetation (NPV)		
3. Non-urban bare surfaces	3.1 Bare soil		
	3.2 Beach		
	3.3 Bare Rock		
4. Water bodies	4.1 Natural/quasi-natural water bodies		
	4.2 Swimming Pools		

Table 3. Land cover classification scheme used for building a spectral library of urban materials (From Herold, 2004).

1. Spectral Variability (and Previous Work)

Surfaces in the urban environment are subject to a variety of conditions that can affect their spectral response. Surfaces used for transportation such as asphalt roads and concrete sidewalks seem to be spectrally similar to the naked eye, but variability can be seen in spectral analysis due to many factors. Wear occurs with increased use of the surface, which exposes layers beneath the top sealant. Asphalt is composed of aggregate, small rocks, and tar or oil along with other hydrocarbons. As asphalt ages, the dark sealant wears down and reveals aggregate that is composed of any number of minerals. New parking lots have a relatively low reflectance and typically no significant absorption

features. Figure 10 shows fresh asphalt having the lowest overall reflectance values and old asphalt in poor condition having the highest overall reflectance values (Herold, 2004). A reflectance peak typically occurs for asphalt in the SWIR at approximately 2100 nm along with prominent absorption features at approximately 2350 nm. Concrete has similar reflectance differences with age, except as concrete ages, the overall reflectance decreases. Herold (2004) suggest that this is caused by the oxidation of the surface, shown by the absorption features in the visible and NIR regions as well as the accumulation of dust and dirt that will decrease the brightness of the surface. Herold (2004) shows spectral variability in various ages of concrete and asphalt (Figure 10).

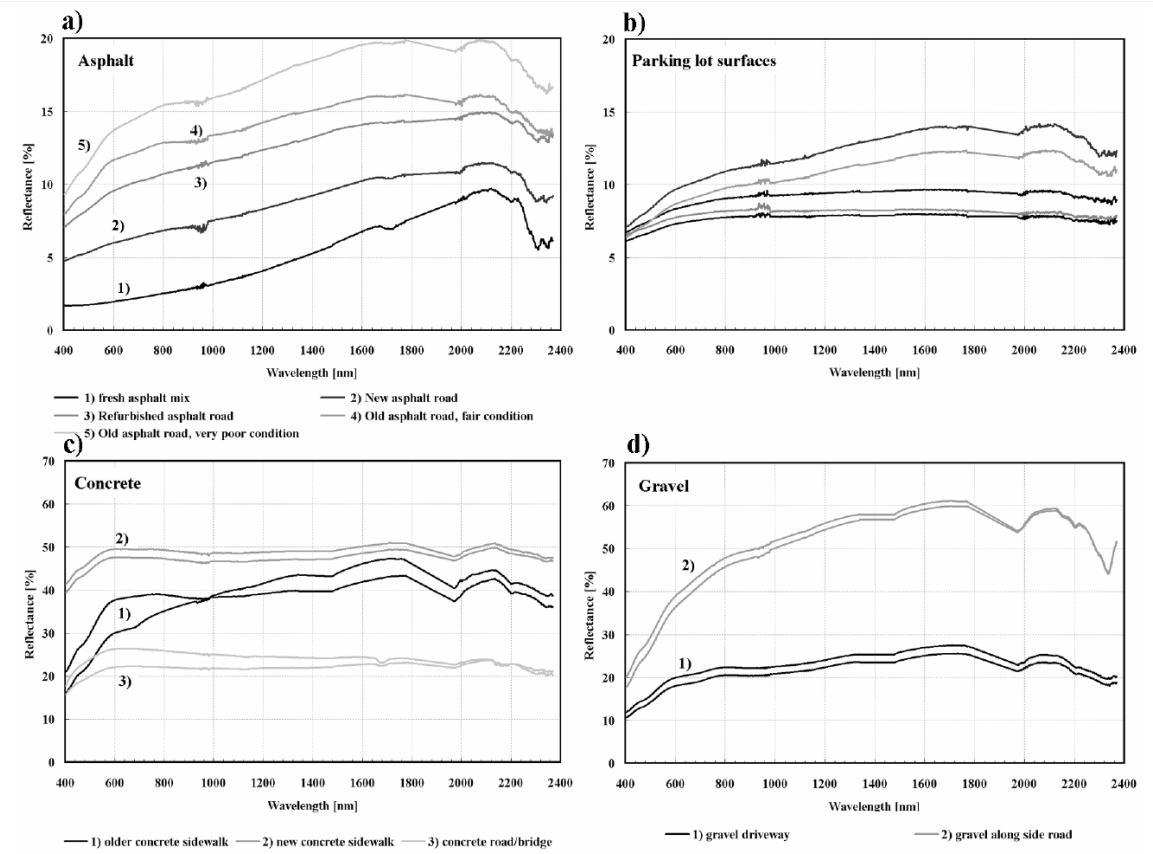

Figure 10. Spectra of asphalt, concrete, parking lot surfaces, and gravel. This figure clearly shows spectral variability as a function of age and/or wear. Asphalt has an overall increase in reflectance with age and concrete has an overall decrease in reflectance with age.

Nasarudin and Shafri (2011) did a similar study on the development of a spectral library for urban remote sensing and also did some analysis on the spectral variability of urban materials. Figure 11 shows the spectra plotted for several urban materials used in the study. An interesting spectrum acquired for this study is polycarbonate. Nasarudin and Shafri (2011) suggested that the overall decrease in reflectance of polycarbonate is caused by the increased transparency of newer materials and that the older materials have a rougher surface, which causes higher reflectance.

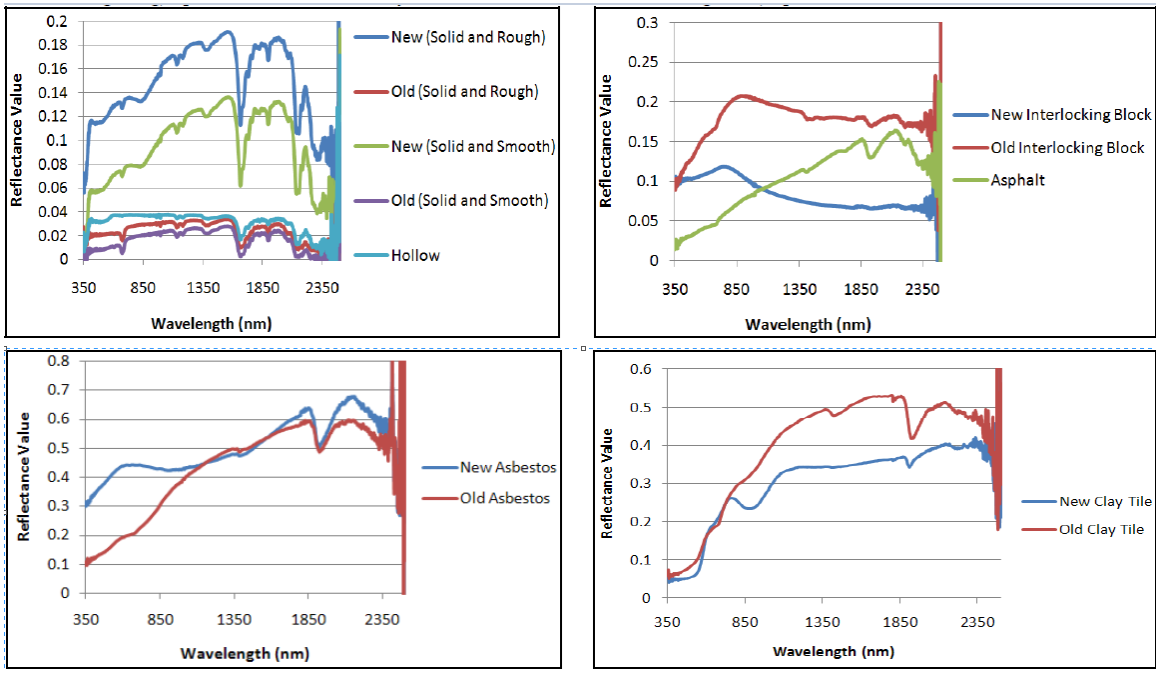

Figure 11. Selected spectra showing spectral variability in urban materials (Nasarudin & Shafri, 2011). Polycarbonate, interlocking block and asphalt road surfaces, asbestos, and clay roof tiles are shown.

While not the topic of this investigation, vegetation also plays an important role in urban environments. Like many forested areas, vegetated portions of urban areas are composed of many species of trees, shrubs, grass, and other plants. Spectral features are typically caused by the plant pigments, cell structure, and moisture content (McCoy, 2005). Chlorophyll, a photosynthetic pigment, typically causes absorption features on

either side of the 550 nm reflection region. When chlorophyll production slows because of plant stress, the depth of the absorption features will decrease and cause the shift in the "red edge" (Figure 12).

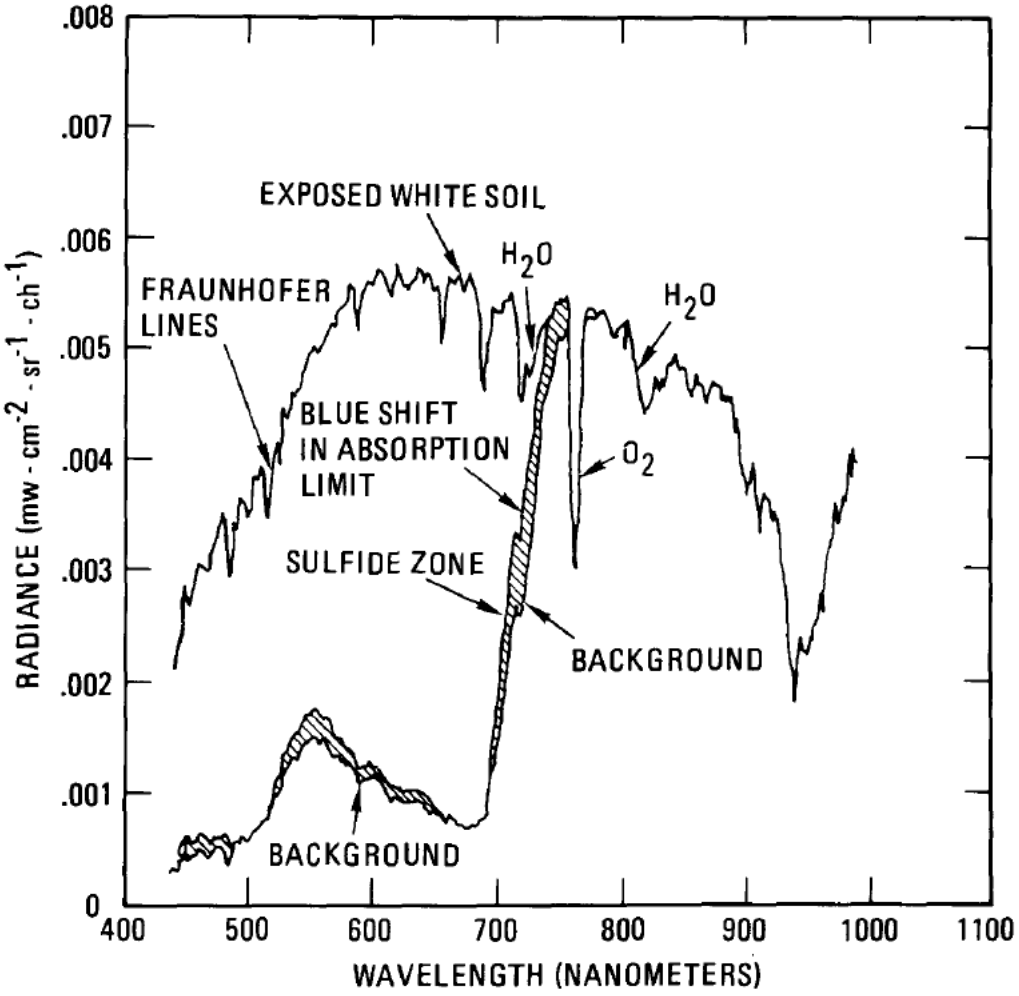

Figure 12. Vane & Goetz (1988) plot of spectra showing variability in vegetation. The steep rise at 750 nm is referred to as the "red edge." The shaded region indicates the 7–10 nm shift to shorter wavelengths caused by geochemical stresses.

Zhang, Rivard, Sánchez-Azofeifa, and Castro-Esau et al. (2006) did an extensive study using HYDICE hyperspectral imagery of tropical tree species in Costa Rica. Intra- and inter-class variability were analyzed using the spectral angle to quantify variability. This study is a good analog for remote sensing of built up urban materials as well as

remote sensing of the urban forest because of the focus on variability within and between classes of materials. In a study that took into account vegetation geometry, Zhang and Qiu (2012) were able to use LiDAR data to detect individual tree crowns, then identify the tree species using hyperspectral data and a specialized algorithm.

THIS PAGE INTENTIONALLY LEFT BLANK

III. METHODOLOGY

A. STUDY AREA AND DATA

1. Naval Postgraduate School Campus

The Naval Postgraduate School in Monterey, California (approximately 100 miles south of San Francisco), is an ideal place to conduct an urban remote sensing study. The campus is situated on the grounds of the historical Del Monte Hotel (opened in 1880) and has an assortment of large and small buildings with a variety of roofing types and ages (Figure 13). The historical buildings and the Del Monte Hotel have various types of clay roof tiles and the newer buildings have an assortment of roof tiles, solar panels, and painted concrete. The campus has concrete, brick, and bare earth walking paths. There is, however, relatively low uniformity to the types of concrete used throughout the campus, resulting from many decades of renovations. This is one reason concrete was used as a case study for this research. Relatively dense vegetation of various species as well as an assortment of ground cover vegetation is found throughout, but the majority of built up urban materials is found in the Northwest corner. Lake Del Monte covers the majority of the Northeast corner of the campus. There are a variety of recreation surfaces ranging from tennis courts to baseballs fields. This thesis focuses primarily on urban built up land cover classes but it would be beneficial to collect spectra that represent the other land cover types found at NPS for further research. A false color image (Figure 13) shows the four major feature classes: vegetation, clay tile, asphalt, and synthetic high reflectance materials.

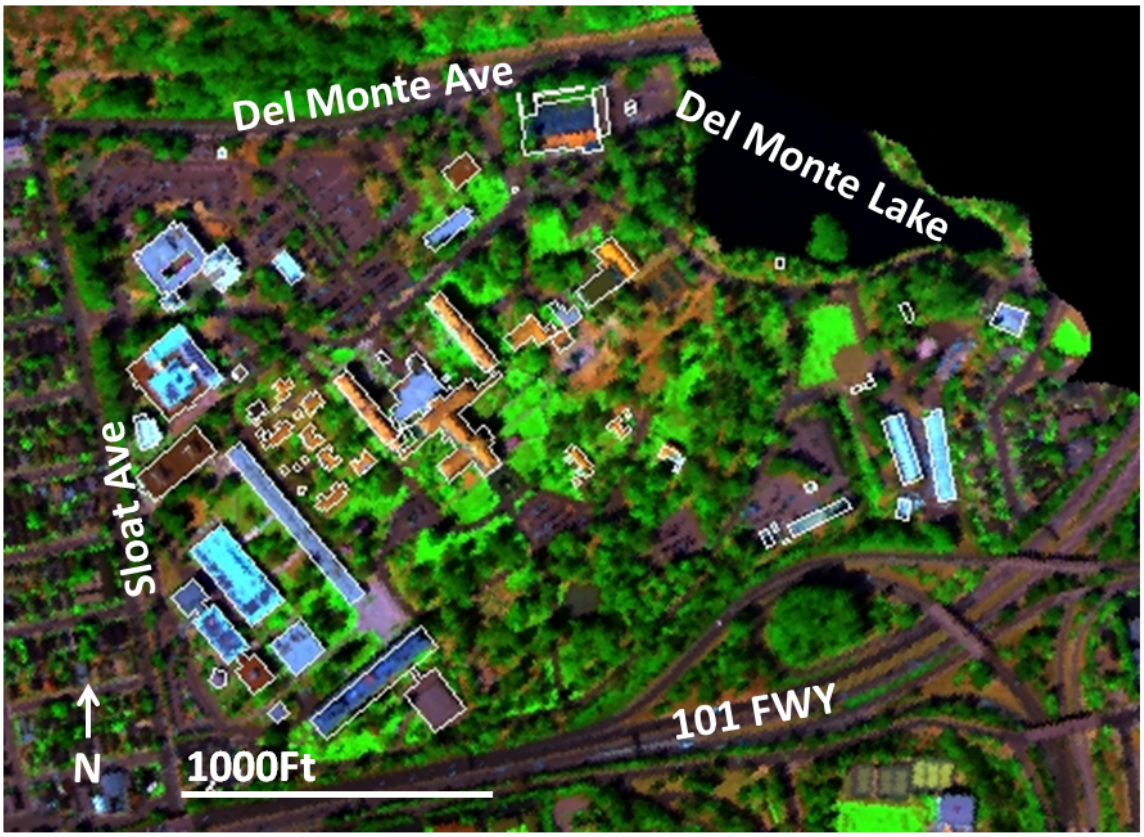

Figure 13. False color AVIRIS image of the NPS campus and surrounding area. Buildings are outlined in white. Spectral bands were chosen to emphasize the predominant materials (Red: 2330 nm; Green: 840 nm; Blue: 430 nm). Vegetation appears green, asphalt is dark gray, clay tile roofs appear orange, and the newer buildings with modern synthetic or painted materials appear blue.

B. SPECTRAL LIBRARY ACQUISITION AND PROCESSING

1. ASD Spectrometer

Several factors were considered when selecting the appropriate field spectroradiometer. Portability is a key factor in doing field collections in the urban environment. The Remote Sensing Center, Naval Postgraduate School, has access to several field spectrometers. Three systems were available at the time of collection (ASD FieldSpec 3, ASD FieldSpec 4, ASD HandHeld 2). Although much more portable than the others, ASD HandHeld 2 was not used because of its lack of bands in the SWIR region. Initial spectral measurements for this research were made using the Fieldspec 3,

but because a Fieldspec4 became available (newer technology), the entire set of measurements were then made with that instrument for consistency.

The ASD FieldSpec 4 Standard-Res Spectroradiometer is a state of the art field spectrometer that allows spectral measuring and viewing in real time, enabling the user to easily assess the spectral signatures and judge the data quality. Its spectral range is from 350–2500 nm using three separate detectors (VNIR 350–1000 nm, SWIR1 1000–1800 nm, SWIR2 1800–2500 nm). The VNIR detector is a 512 element silicon array capable of 3 nm spectral resolution and 1.4 nm sampling interval. The SWIR1 and SWIR2 detectors are a graded index indium gallium arsenide (InGaAs) photodiode capable of 10 nm spectral resolution and 2 nm sampling interval. The spectroradiometer is controlled with a windows laptop via Wi-Fi. Coordinates of each collection site are provided via a Bluetooth connected GPS antennae. The instrument is factory calibrated for wavelength, absolute reflectance, radiance, and irradiance (National Institute of Standards and Technology traceable). It includes a backpack and a laptop strap that enables a single person to collect spectra without assistance (Figure 14). The ASD contact probe provides halogen lighting over approximately 1 cm diameter FOV.

Figure 14. Photograph of typical ASD spectrometer configuration showing spectra being collected using a contact probe (with broom handle extension). FieldSpec 4 spectrometer unit is contained in the backpack. The fiber optic cable and power cable for the contact probe are seen.

In operation, the spectrometer is allowed to warm up prior to use for at least 30 minutes to allow the sensors to become stable. There are three sensors spanning the VNIR/SWIR and each stabilizes at a different rate; therefore, improper warm up procedures will result in spectra with large spikes between the 1000 and 1800 nm regions (small spikes are expected and accounted for with post processing). Instrument parameters are then set accordingly. For use with the contact probe foreoptic, bare fiber (25 degree FOV) is chosen. The instruments gain settings are then optimized while the foreoptic is measuring the Spectralon panel to account for over-saturation of the SWIR detectors. Optimization is performed every hour, when lighting conditions change, if for any reason the instrument has to be restarted, or if changes in temperature occur. Time between optimization and gain settings are recorded in the header file.

As stated before, spectra are recorded in the raw form as radiance in digital numbers (DN) units. There are two ways to go about converting the DNs to reflectance and both have advantages and disadvantages. The first method requires recording all spectra as radiance while also collecting and saving radiance measurements of the Spectralon panel between measurements or when lighting conditions change (Figure 15).

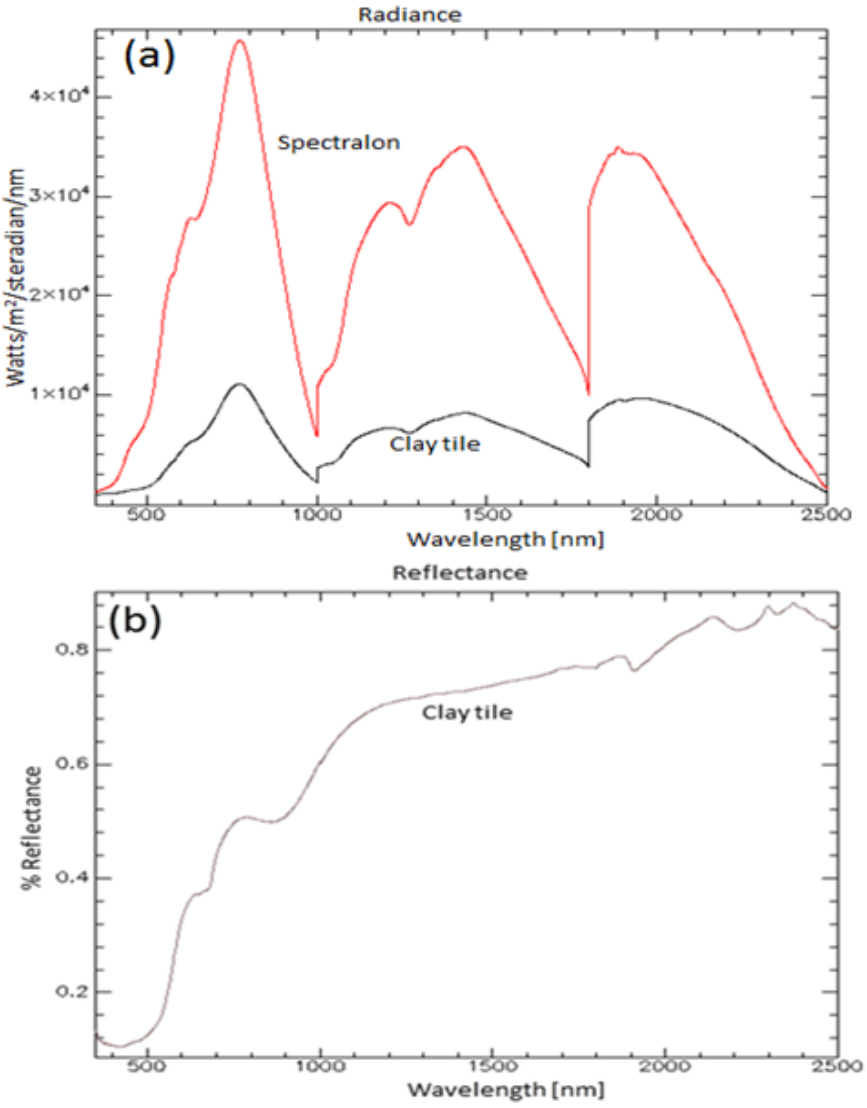

Figure 15. (a) Spectralon and clay tile radiance measurement used to calculate apparent reflectance. (b) Reflectance spectrum of a clay roofing tile.

Converting to reflectance during post-processing is advantageous in that any collection issues can be tracked back to either the sample collection or the Spectralon measurement, but not advantageous in that more post processing is required. The second method is more automated and for an inexperienced spectral scientist, more efficient. The white balance (WB) is measured and saved internally using the Spectralon panel as a standard. This measurement is applied to all spectra recorded after WB is performed and real time reflectance measurements are made possible. Radiance measurements are still saved between every few samples, yet these are not needed unless issues are found in the data. The instrument configuration setting can control the number of spectra to be averaged internally per sample as well as dark current and white reference measurements used for calibration.

Spectra may now be collected after warm up procedures, optimization, and WB/Spectralon measurement. A base name is chosen that represents the class of materials being sampled. The base name will follow the spectrum through post processing and into the spectral library therefore it is important to pick a base name that is short and descriptive. The "number of files to save" setting is primarily used when covering a large area with the pistol foreoptic then averaged, but is used in this study to collect multiple spectra within the same area. Because FOV and lighting conditions will not change between each file when using the contact probe, all spectra for a given sample should not deviate much. More detailed comments can be made on a field report but a short comment will be saved in the header of the spectra file.

An efficient sampling strategy that was conducive to building a comprehensive spectral library was extremely important to this research. At first, spectra of all classes were collected together, without much forethought into how they would be grouped into the library or contribute to the research. It was determined to be more efficient to collect spectra of an entire class of materials during the same day, then process it all at the same time. Because this thesis is mostly focused on looking at the intra-class variability of urban materials, more emphasis was put on collecting spectra of each class than compiling a large library of the various material classes.

There are many more restrictions for collecting spectra with the pistol grip (natural light) than using the contact probe; therefore only spectra that were collected using the contact probe were included in the library used for analysis. The contact probe allows full control over-lighting and FOV. The urban environment is very complex spatially and spectrally and full control over the FOV allows a much more precise study of the materials that make up the surface (Figure 16).

Figure 16. Various urban materials at NPS showing spectral variability within the FOV of a typical pistol grip foreoptic. Using the contact probe, each individual component is sampled. (A) Heavily worn asphalt with road paint (B) Two types of concrete with plastic border (C) Concrete with brick squares (D) Various clay roof tiles.

Most of the first spectra measured were discarded due to a lack of metadata and or issues with operating the spectrometer. With direct sunlight, it is difficult to see the laptop screen and qualitatively judge whether the spectra have quality issues, therefore there were many issues with the first spectra that were not found until they were processed. The spectrometer is a complicated instrument with many settings and

parameters that need to be set accordingly. Although there are many resources for learning how to operate the spectrometer, trial and error seems to be the most effective learning method (with the exception of errors that might damage the spectrometer).

The NPS campus is a large area to survey on a point basis; therefore it was necessary to create a plan of attack in collecting spectra. The campus was surveyed by walking the grounds and using high resolution imagery to assess what types of materials are present, then land cover classes were recorded. To assess the types of materials present at NPS, a spreadsheet was created that noted each feature (i.e., parking lot, building) and attributed the feature with a description of the type of material, the condition of the material, and the percentage that that material covered the feature being described (Table 4).

Location/Building #	Material	% of area	Comments
Parking Lot A1	weathered asphalt	100	All asphalt appears same age, white lines
Parking Lot A2	weathered asphalt	100	All asphalt appears same age, white lines
Parking Lot B	weathered asphalt	100	All asphalt appears same age, white lines
Parking Lot C	weathered asphalt	100	All asphalt appears same age, white lines
Parking Lot D	weathered asphalt	100	All asphalt appears same age, white lines
Parking Lot E	fresh asphalt	100	Asphalt is dark black, white lines are bright
Parking Lot F	weathered asphalt	100	All asphalt appears same age, white lines
Parking Lot G	weathered asphalt	100	All asphalt appears same age, white lines
Parking Lot H	khaki paving brick	100	Standard-size paving bricks, white lines
Parking Lot I1	weathered asphalt	100	All asphalt appears same age, white lines
Parking Lot I2	khaki paving brick	100	Standard-size paving bricks, white lines
Parking Lot I3	khaki paving brick	100	Standard-size paving bricks, white lines
Parking Lot J1	weathered asphalt	100	All asphalt appears same age, white lines
Parking Lot J2	weathered asphalt	100	All asphalt appears same age, white lines
Parking Lot J4	weathered asphalt	100	All asphalt appears same age, white lines
Parking Lot J3	weathered asphalt	100	All asphalt appears same age, white lines
Parking Lot J4	weathered asphalt	100	All asphalt appears same age, white lines
Parking Lot J5	weathered asphalt	100	All asphalt appears same age, white lines
Parking Lot J6	weathered asphalt	100	All asphalt appears same age, no lines
Parking Lot J7	weathered asphalt	100	All asphalt appears same age, white lines
Parking Lot J8	weathered asphalt	100	All asphalt appears same age, white lines

Table 4. Sample of the campus survey form used to assess the materials that need to be measured. An estimate of the percentage covered by the dominant material is given.

Spectra were then collected using the ASD spectrometer according to the spreadsheet plan. Table 5 shows a second spreadsheet used to record actual spectrum collection parameters, location, and spectral quality assessments. Figure 17 shows the

locations of spectra measured and illustrates the spread of spectrum collection data points using GPS data from the spectrometer. The original plan was to walk each roof top and collect spectra of roofing material but rooftop access was limited, therefore it was difficult to collect spectra from some buildings. This thesis is a component of larger project that will include a comprehensive spectral library of most materials on campus. Approaches, methods, and recommendations from this thesis will help guide this effort.

file name	comments	lat	long	quality	avg	unit
sidewalk 00001	very dirty concrete	36.59834	-121.872	good	no	fieldspec4
sidewalk 00002	very worn and old coarse aggregate, various rocks	36.59809	-121.872	good	no	fieldspec4
sidewalk 00003	painted white concrete, newer paint, low roughness	36.59809	-121.872	good	no	fieldspec4
sidewalk 00004	red paint on concrete, newer paint, slightly rough	36.59809	-121.872	good	yes	fieldspec4
sidewalk 00005	red paint on concrete, newer paint, slightly rough	36.59809	-121.872	good	yes	fieldspec4
sidewalk 00006	grey paint on concrete, slightly rough, new paint	36.59809	-121.872	good	no	fieldspec4
sidewalk 00007	very smooth light color concrete, new, no wear	36.59785	-121.873	good	no	fieldspec4
sidewalk 00008	older dirty concrete, worn, small aggregate	36.59785	-121.873	good	no	fieldspec4
sidewalk 00009	very old worn concrete, rough texture,various rock	36.59785	-121.873	good	no	fieldspec4
sidewalk 00010	reddish concrete, very smooth, little wear	36.59785	-121.873	good	no	fieldspec4
sidewalk 00011	very old,worn,dirty,oxidized,various rocks	36.59687	-121.873	good	no	fieldspec4
sidewalk 00012	rough,old,some moss growth	36.59678	-121.872	good	no	fieldspec4
sidewalk 00013	old bricks,red, dirty	36.59682	-121.872	good	yes	fieldspec4
sidewalk 00014	old bricks,red, dirty	36.59681	-121.872	good	yes	fieldspec4
sidewalk 00015	old bricks,red, dirty	36.59678	-121.872	good	yes	fieldspec4
sidewalk 00016	old bricks,red, dirty	36.59678	-121.872	good	yes	fieldspec4
sidewalk 00017	old bricks,red, dirty	36.59679	-121.872	good	yes	fieldspec4
sidewalk 00018	old bricks,red, dirty	36.59682	-121.872	good	yes	fieldspec4
sidewalk 00019	old bricks,red, dirty	36.59684	-121.872	good	yes	fieldspec4
sidewalk 00020	compacted, smooth, dirt path, slightly wet, brown	36.59628	-121.872	good	yes	fieldspec4
sidewalk 00021	compacted, smooth, dirt path, slightly wet, brown	36.5963	-121.872	good	yes	fieldspec4
sidewalk 00022	compacted, smooth, dirt path, slightly wet, brown	36.59628	-121.872	good	yes	fieldspec4
sidewalk 00023	newer, slightly rough, light color concrete	36.59615	-121.873	good	yes	fieldspec4

Table 5. Table showing a selection of the spectra collected. Comments are consolidated from the field notes to describe the material. GPS coordinates are converted to decimal degrees. All data are manually inspected for issues and commented on; whether the spectrum is good or if additional measurements are required.

Figure 17 shows the spread of data collection points throughout the campus. GPS locations were recorded for each data point along with a short description of the material. This was very useful when doing analysis of sidewalks since they are less of a discrete surface, as opposed to rooftops or parking lots. Coordinates were recorded with a GlobalSat BT-359 GPS receiver connected to the laptop via Bluetooth. Accuracy was within 10 meters. Map was created with ESRI ArcMap using a high resolution true color image and NPS facilities data for reference.

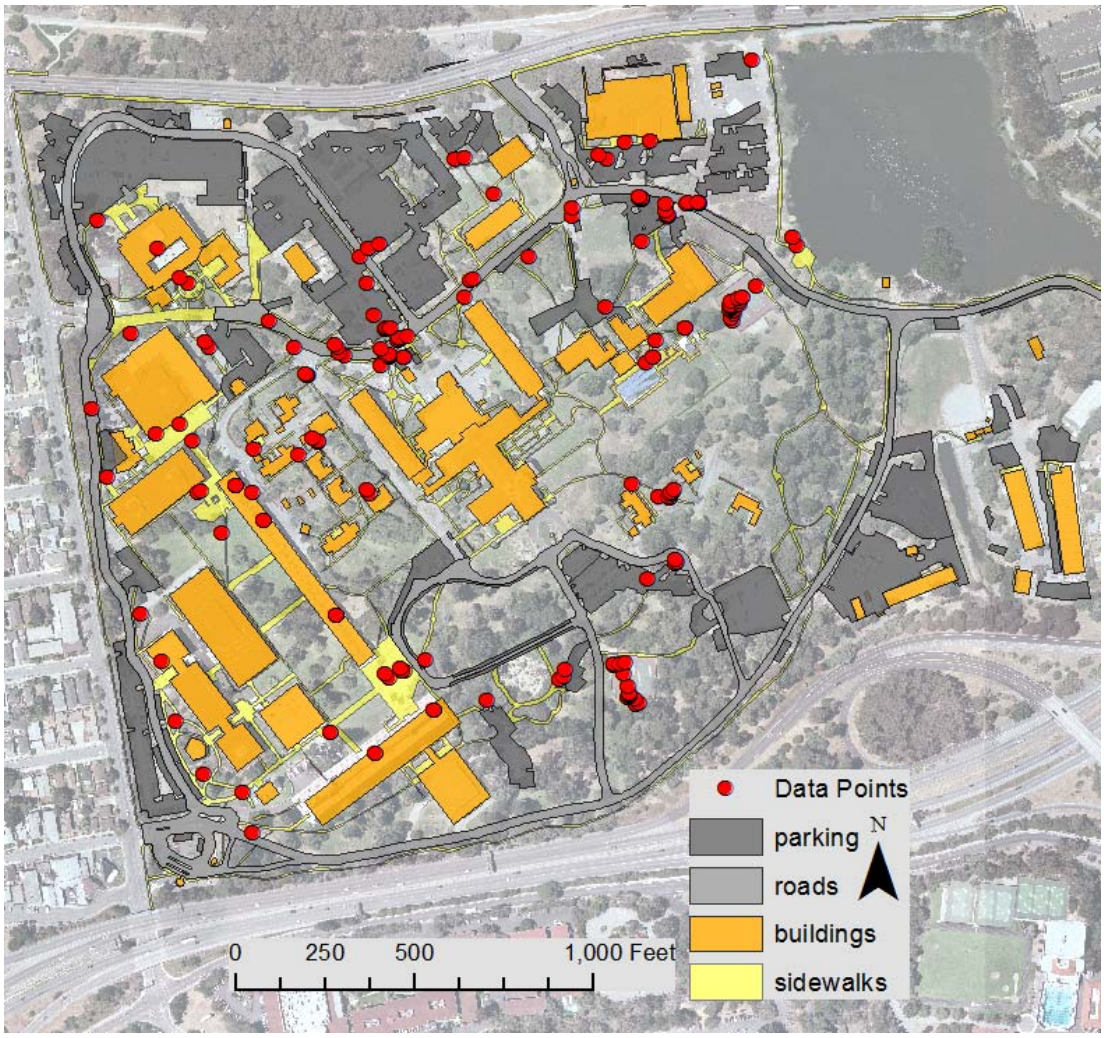

Figure 17. Data collection sites with buildings, sidewalks, and parking lots for reference. Background image used is a high spatial resolution aerial photograph acquired August 12, 2012.

ASD spectra post processing was completed using ASD ViewSpec Pro (version 6.0) software (www.asdi.com). A correction is made to remove offsets between the VNIR and SWIR sensors and a splice corrected (.sco) file is created. The data are then exported as an ASCII file in either DN or reflectance units. The ASCII text files contain a header for the metadata, column for wavelength, and a column for percent reflectance. The ASCII files can be viewed, edited, and compiled using a choice of several software systems; the free software, Spectral Analysis and Management System (SAMS), was used for this research (www.cstars.ucdavis.edu/software/sams/). Before compiling the spectra into a library, each spectrum was reviewed using SAMS for issues. Because several spectra were taken of the same point, theoretically they should all have same spectral curve. Therefore, any spectra that deviated from the mean from that sample were determined to be bad. Some spectra were averaged to represent a larger class of data (i.e., bricks or various colors were averaged into one spectrum). Averaged spectra were labeled with (avg) in the file name allowing the spectra to be traced back to the original notes. SAMS exports the edited ASCII files into ENVI spectral library (.sli) files. Libraries created in this fashion are viewable with ENVI but need to be resampled to match the response of the sensor for the HSI. Because only wavelength are known, ENVI uses a Gaussian model with the full width half max (FWHM) equal to the band spacings. The spectral library can now be used for classification. To prepare the spectral library for use with the AVIRIS data, spectral resampling was performed to resample the data to the AVIRIS wavelength space.

2. Spectral Feature Analysis

Analysis of spectral signatures can help in the discrimination and/or identification of materials. Materials commonly found in the urban environment are composed of a variety of synthetic, natural, and chemically altered natural materials that have no analogue in non-urban environments (Roberts & Herold, 2004). These materials may be altered by weather, age, contaminants, or other factors that contribute to intra-class variability. These spectral features are identifiable by qualitative analysis (visual

comparison) or by algorithms designed to detect specific features. A qualitative analysis can determine what components in the material contribute to the shape of the spectral signature.

A qualitative analysis (spectroscopic analysis) of urban spectral variability involves identifying the absorption features based on their location (bands), and relative depths/widths (full width at half the maximum depth) (Richards, 1999). Urban materials are composed of many materials; therefore identifying spectral features associated with known materials may suggest variability in the composition. The spectral library is analyzed on a per spectrum basis comparing features with other spectra in its class to determine what type of spectral variability is present. The first step in analyzing HSI is to browse the image pixel-by-pixel to get an idea of what the types of materials are represented in the image. To aid in reviewing possible spectral endmembers, Pixel Purity Index (PPI) is performed to determine which pixels are the most spectrally pure (extreme) thereby eliminating spectra that have mixing caused by several materials.

Spectral signatures are defined by their peaks and valleys caused by the materials physical reaction to the various wavelengths in the electromagnetic spectrum. Two processes, electronic and vibrational, are the primary cause of absorption features in materials. Electronic processes are caused by the absorption or emission of photons. Absorption of photons at a specific wavelength causes energy to change from a low state to a high state; emission is the opposite. Mineral identification is often made possible by the absorption features in the spectra caused by the crystal field effect. Unfilled electron shells of transition elements (i.e., Ni, Cr, Co, Fe) are split when the atom is located in a crystal field which causes a change in energy from low to high by absorption of a photon having matching energy difference between the states. The various structures of crystal fields make identification of minerals possible by identifying the absorption (Clark, 1999).

Continuum removal of spectra normalizes reflectance, thereby allowing analysis of individual absorption features from a common baseline. The continuum curve is fit over the top of the spectrum by connecting local spectra maxima by straight-line segments. Spectra from the urban spectral library are compared to other spectral libraries

(i.e., USGS mineral library) as well as spectra from the AVIRIS imagery to determine the variability of spectral features. Because all spectra collected from the library represent approximately one square cm, spectra are averaged to better determine their spectral contribution to imagery spectra. This is done in ENVI with spectral math simply by adding the spectra within a class of materials then dividing by the total.

C. HYPERSPECTRAL DATA AND PROCESSING

1. Airborne Visible/Infrared Imaging Spectrometer (AVIRIS)

The AVIRIS data used for this research were acquired on September 30, 2011 aboard a Twin Otter aircraft flying at 10,000 ft. (3,048 m). The sky was clear with a few clouds toward the end of the collection (not within the study area). A subset of the image was used for analysis (Figure 18). Future research may expand to include materials in the greater Monterey region. A subset of 483 x 351 pixels covering the NPS campus was used for analysis. The data had 224 spectral bands covering the spectral region from 400–2500 nm at approximately 2.36 m spatial resolution. While data were provided as corrected reflectance, the full processing chain for these data will be described.

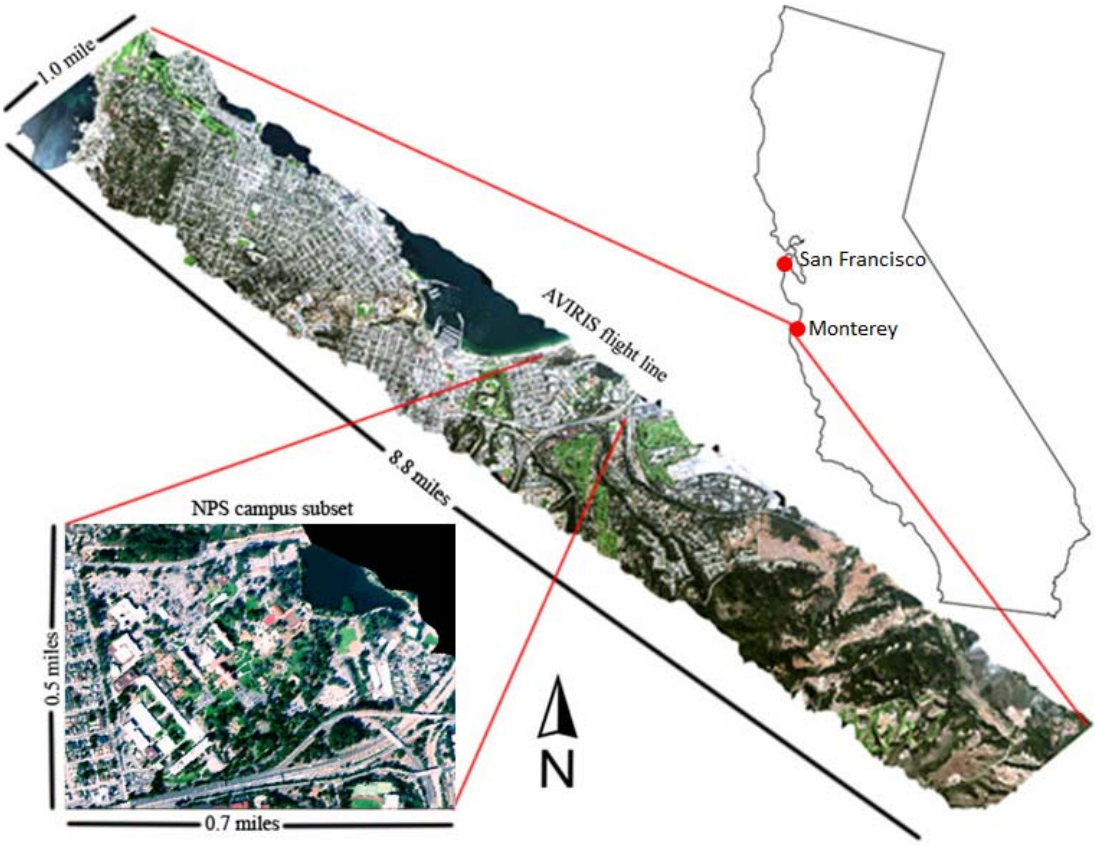

Figure 18. Entire AVIRIS flight line with the spatial subset of the Naval Postgraduate School Campus.

2. Radiometric Corrections

AVIRIS imagery is provided as calibrated radiance data with flight data that can be used to georectify the image to within a few meters accuracy. The data are first atmospherically corrected and converted to apparent surface reflectance using one of the available atmospheric correction software packages available. The two most common software packages are: Atmospheric CORrection Now (ACORN), and Fast Line-of-sight Atmospheric Analysis of Spectral Hypercubes (FLAASH) (Kruse 2004). Both systems use a version of the radiative transfer model:

$$Lsensor_{\lambda}=LSun_{\lambda}T_{\lambda}R_{\lambda}+LPath_{\lambda} \quad (4)$$

where λ is wavelength, $L_{sensor\lambda}$ is the radiance at the spectrometer, $L_{Sun\lambda}$ is the solar radiance above the atmosphere, T_{λ} is the total atmospheric transmittance (product of transmittance from sun to earth and back to sensor), R_{λ} is the surface reflectance at the observational geometry, and $LPath_{\lambda}$ is the path scattered radiance (Gao & Goetz, 1990). Both packages use MODTRAN4 technology to produce surface reflectance without ground measurements. A single reflectance spectrum from a ground targets can be used to minimize artifacts that flank the water vapor bands and compensate for measured and modeled radiance (Figure 19) (Roberts & Herold, 2004). ACORN was used for preprocessing of the AVIRIS data and beach sand was used as a ground target (Kruse et al., 2012).

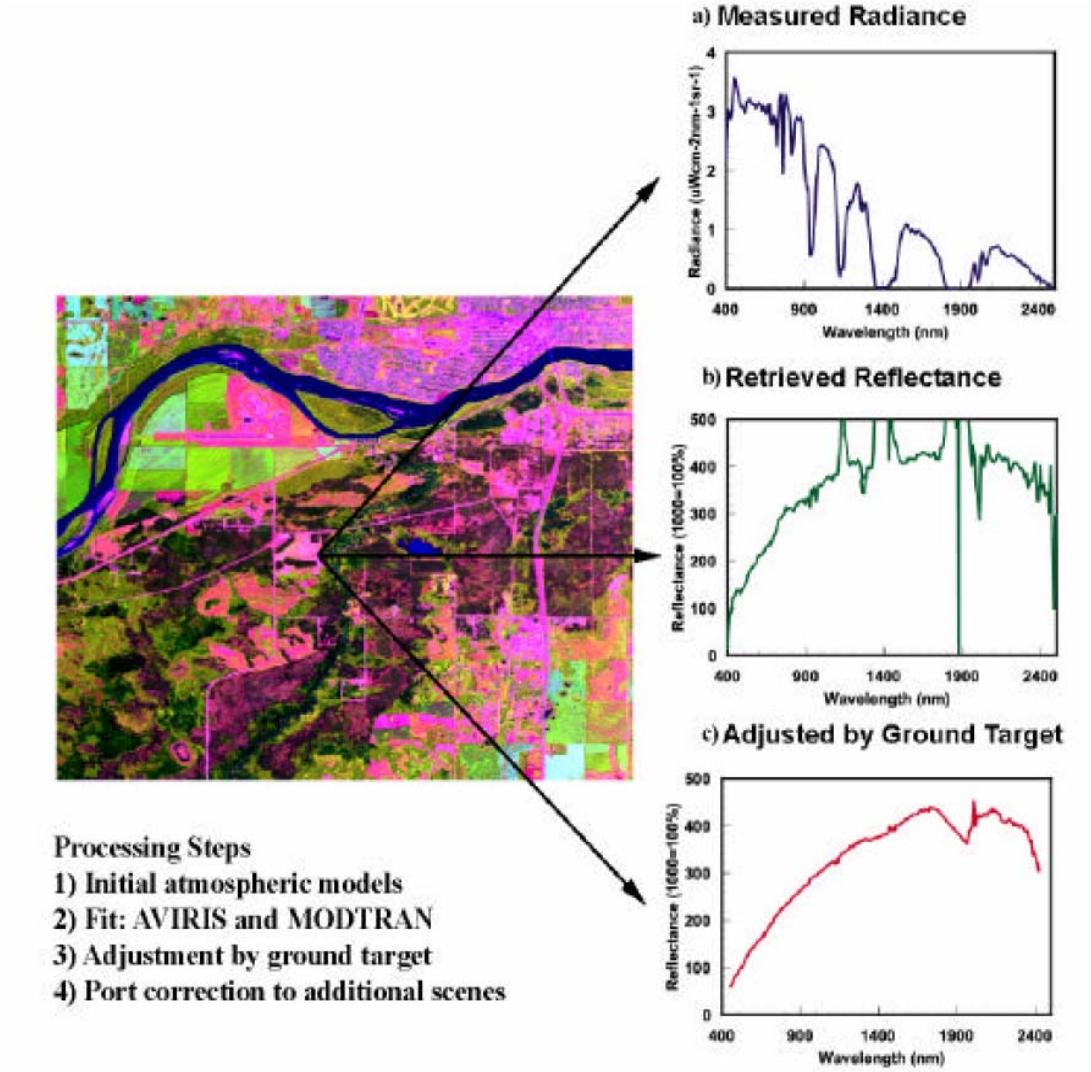

Figure 19. Atmospheric correction steps required for HSI analysis (Roberts & Herold, 2004)

3. Vegetation Removal

Because this thesis is focused on non-vegetative materials, vegetation was masked from the study area prior to analysis. The normalized difference vegetation index (NDVI) is the most common vegetation identifier and was determined to be adequate for this research. The NDVI equation uses the difference between the NIR region (high in vegetation) and the red region of the spectrum (low in vegetation) to create an index (0–1) with higher values corresponding to vegetation (Olsen, 2007).

The trial and error method was used to decide what threshold to use to capture enough vegetation to unclutter the image but allow pixels that may be mixed with spectra of interest to remain. Vegetation will not be confused with any of the urban materials of interest (except in mixed pixels) so a relatively low threshold was used to minimize the loss of any pixels of interest. A region of interest (ROI) was created to be used as a mask for all pixels classified as vegetation. A high resolution true color composite was used to determine if the ROI included any pixels that represent non-vegetative materials. A mask was also created to remove pixels outside the NPS boundaries to better quantify the materials present at NPS.

4. Spectral Discrimination and Classification

There are several algorithms designed to use a spectral library to map the spatial distribution of materials in a spectral library. The Spectral Angle Mapper algorithm (SAM) is a common method used to classify an image based on field spectra and/or endmembers extracted from HSI and typically the first method used because a classification map is automatically produced (other methods require more user input). This thesis uses SAM as a measure of spectral variability as well as classification. The Mixture Tuned Matched Filtering algorithm was used for the final classification of materials because of the algorithm's ability to classify the mixed pixels that are common in the urban environment.

SAM works in N dimensional space where the pixel vector x is defined by its angle measured with respect to the axes that define the coordinate system of the space rather than the magnitude (length) of the vector (Richards, 1999). A maximum angle (in radians) is set to determine the threshold to what will be considered a particular material. When mapping multiple endmembers, it is possible to select multiple values to account for classes of materials that require a higher or lower threshold to be classified.

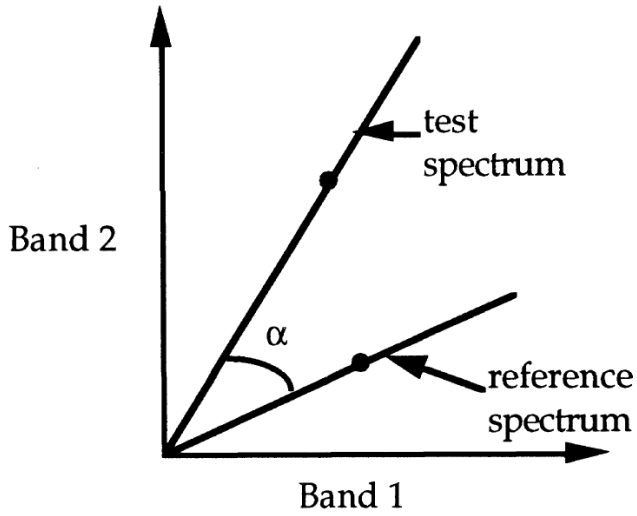

Figure 20. Spectral Angle Mapper (SAM) represents pixels or reference spectra based on their angles from the band axes. This plot is simplified to represent a two-band image with a test spectrum and a reference spectrum (From Kruse et al., 1993)

For this research, spectral endmembers were chosen from various classes in the AVIRIS imagery that represent classes identifiable in the imagery (i.e., roof types, asphalt, concrete). These classes are used primarily for inter-class variability analysis because field spectra (using the contact probe) better represent intra-class variability. The spectral angle threshold between the test spectrum and the reference spectrum is chosen based on how similar other spectra are to the reference spectrum. Materials with spectra that are unique to the study area or materials of large classes generally can use larger angles to map all the materials in the image. Materials such as various red tile roofs require a smaller angle to account for the low variability between similar tile types. A SAM classification image is created by selecting "multiple values" when entering the SAM parameters.

Classification using SAM and library spectra was performed in the same way, but a classification image was created for each class rather than all classes in one image. Because spectra collected in the field represent very extreme pixels due to the small spatial area (1 cm^2) each field collection represents, spectra were averaged to better represent a larger FOV (approximately 2.3 meters). This could also be accomplished with

a larger FOV foreoptic used with the field spectroradiometer but intra-class variability would not be as evident as if spectra from each material were analyzed individually.

The Mixture Tuned Matched Filtering algorithm was used to quantify the abundance of urban materials. MTMF requires a considerable amount of pre-processing and conditioning of the data to produce a classification result with minimal false positives. The first step of pre-processing and data conditioning is to perform a minimum noise fraction (MNF) transform. Application of an affine transform to the original data characterizes, decorrelates, and whitens any noise in the data, therefore allowing a quantitative estimation of detection probability. Matched filtering (MF) and mixture tuning (MT) may be performed once the image data and target spectrum are in MNF space. Matched filtering is used for detecting a target signature within mixed pixels of an unknown background by using a linear detection method. Mixture tuning detects false positives within the MF images (infeasible mixtures), therefore reducing the number of false positives (Boardman and Kruse, 2011). A 2-D scatterplot of MF versus MT is produced to map pixels that have a high MF score and a low infeasibility score. These pixels are saved as a region of interest and used for classification.

THIS PAGE INTENTIONALLY LEFT BLANK

IV. RESULTS

A. RESULTS AND DISCUSSION

1. Visual Analysis of Study Area

A high resolution aerial photograph was used to assess what materials are spectrally unique in the VIS and to get a good idea of features in the image that may affect classification. Figure 21 shows a close up of a portion of the NPS campus that contains a variety of urban materials that were further investigated using AVIRIS imagery as well as field spectral measurements. Buildings discussed are labeled in Figure 21. At least three types of clay tile roofs are used on the historical buildings (i.e., Hermann Hall: "H," and the quarters "G"). The materials on the tile roofs are relatively homogenous compared to the roof of the building on the lower left (Root Hall: "F"). The main roofing material used for Root hall appears to be highly reflective and with many smaller features throughout the center of the roof. Asphalt on roads and in parking lots (grey in Figure 21) looks relatively homogenous overall, with clear signs of use (darker areas assumed to be from oil or other contaminates) in high traffic areas. White road paint is used throughout most of the roads and parking lots. Sidewalks are all relatively high in reflectivity and are mostly bordered and obstructed by vegetation. The term over- and under-classified is used to refer to classification where classification caused false-positives (over-classified) or failed to classify pixels within the intended class (under-classified).

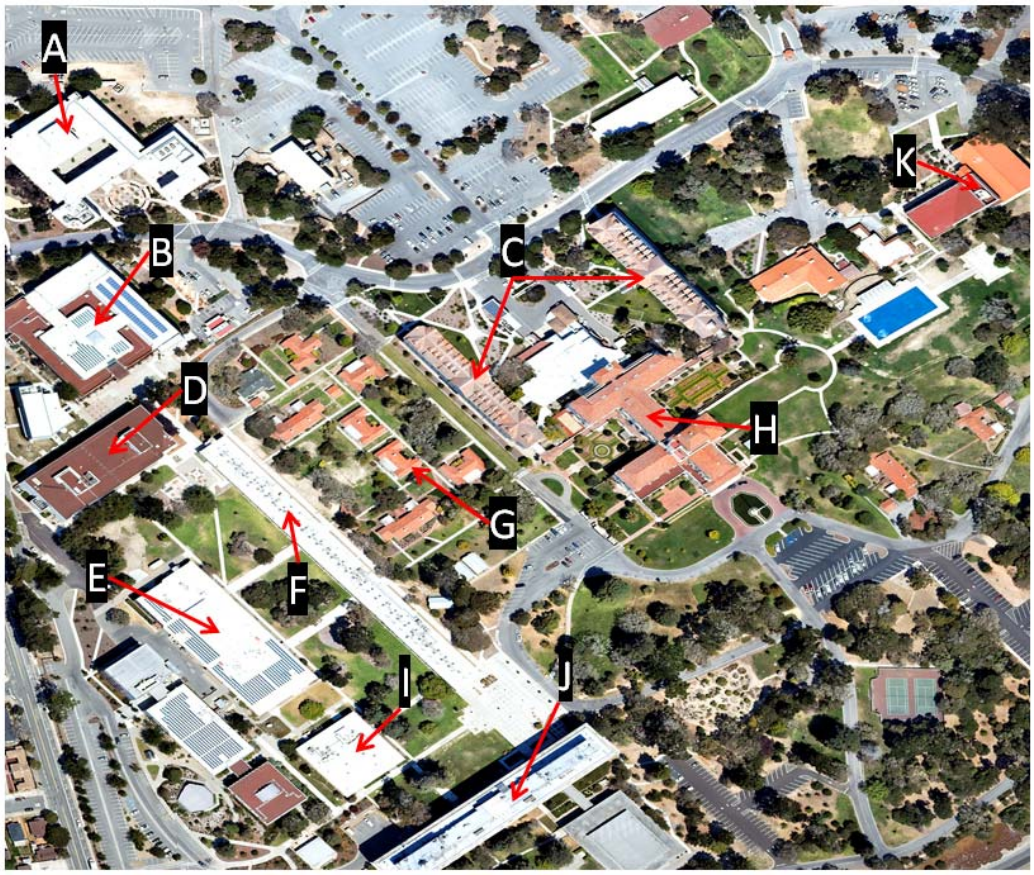

Figure 21. High spatial resolution aerial photograph acquired August 12, 2012. (A): Glasgow Hall. Flat roof, mostly synthetic roofing material with a courtyard in the center (B): Library. Red gravel used to cover the synthetic roof on the south west periphery. Majority of roof is synthetic roofing material combined with solar panels and various air conditioners and other objects. (C): Hermann Hall wings. East and West wing are identical. Complicated geometric roof covered with light colored clay tiles. (D): Ingersoll Hall. Red gravel roof with various air conditioner units throughout. (E): Halligan Hall. Flat synthetic roofing materials with solar panels covering the South and East sides. (F): Root Hall. Primarily synthetic roofing material with skylights and air conditioner units down the center. (G): "Quarters." Various small buildings scattered throughout the campus. Clay tile roofs with varying degrees of algae growth, oxidation, and tree droppings. (H): Hermann Hall main building. Primarily orange clay tiles with a few non-tile objects throughout. Synthetic roof material used for the northern end of the building. (I): Bullard Hall. Synthetic building materials with air conditioner units throughout. (J): Spanagel Hall. Primarily grey non-skid paint over concrete but cluttered with various antennas, and air conditioner units. (K): Fitness Center. Clay tiles used for east end roof and red gravel used for the flat West roof.

2. Vegetation Masking

The NDVI image (Figure 22a) was used to determine which materials are non-vegetative. The NPS campus (including the lake) is 50% vegetation. Urban/Water: 45296 pixels; Vegetation: 44413 pixels. The AVIRIS image has a spatial resolution of 2.3 meters therefore many of the pixels corresponding to smaller roads, paths, or sidewalks that have vegetation overhang or bordered by vegetation may be classified as vegetation if too high of threshold is used. Figure 22b shows the mask derived from the NDVI image. This step is necessary to declutter the image and allow improved classification of urban materials.

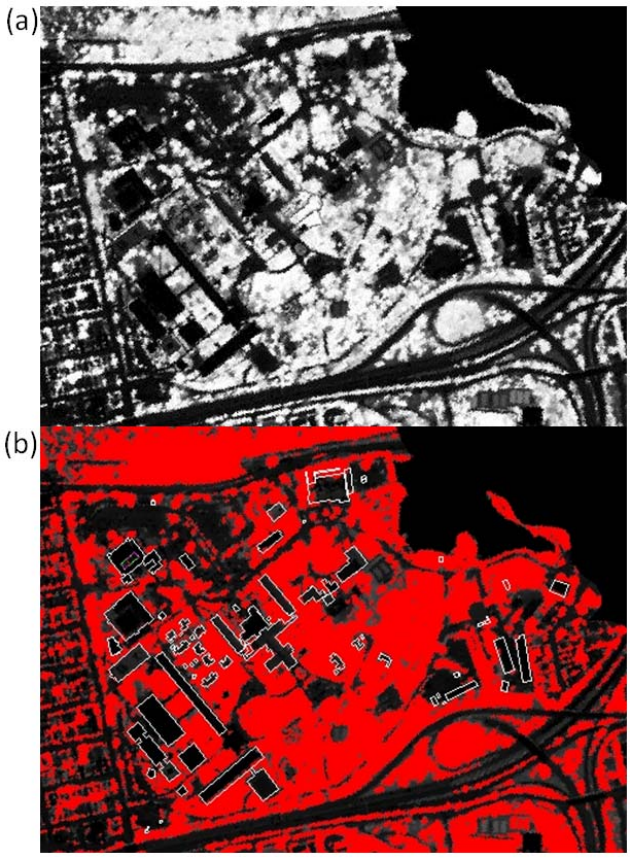

Figure 22. (a): NDVI image shows vegetated areas as brighter pixels. (b): Red pixels show the Region of Interest (ROI) that corresponds to any pixel with an NDVI value of 0.3 or above. The threshold value was determined to be vegetation by visual comparison to a true color composite image. Anything below a 0.3 NDVI value was determined to be a non-vegetative material. Buildings are outlined in white for reference.

3. Clay Tile

Clay tiles are used for the roofs of most of the historical buildings at NPS. Clay tiles are composed of clay minerals, quartz, and ferric oxides (Heiden, 2001). The tiles are fired, colored with various materials that contribute to their spectral variability. Much of the spectral variability is caused by the builder using tile of different colors for aesthetic purposes (Figure 23) but variability is also caused by age, and fouling (i.e., moss, lichen, oxidation).

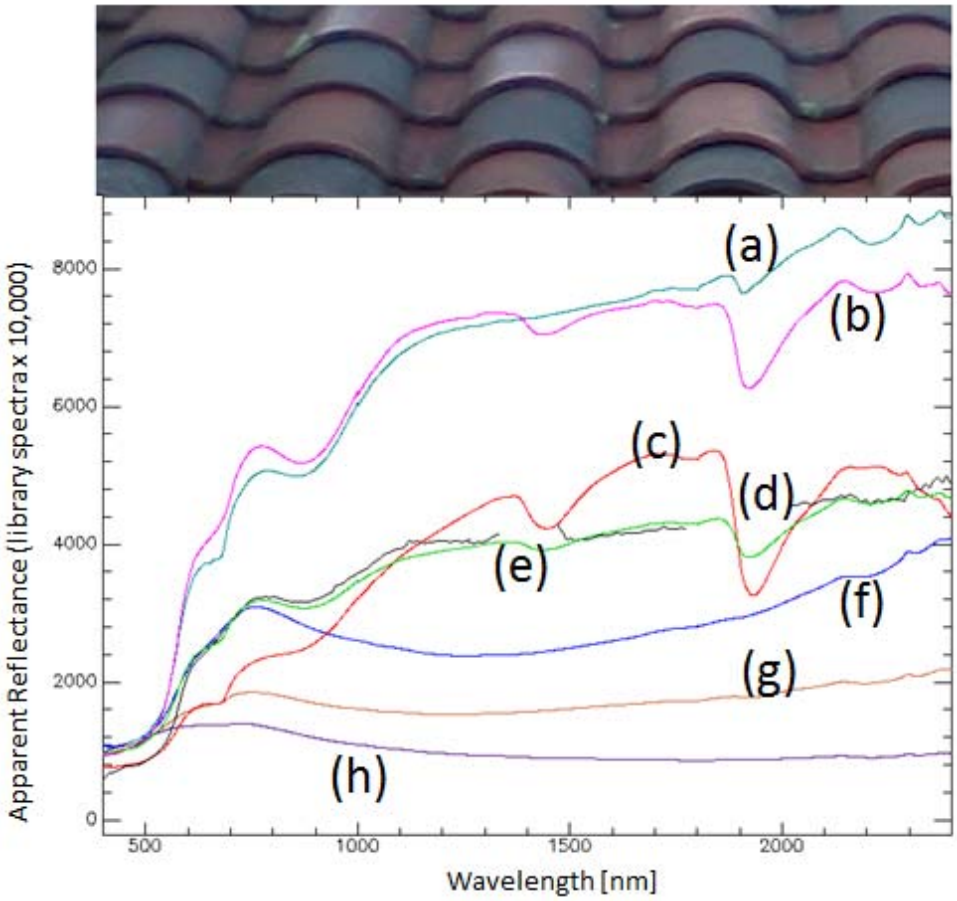

Figure 23. Spectra used for classification of clay tile roofs. Top: Photograph of the clay tiles showing the spectral variability of the materials. Bottom: Spectra of various roof tiles. All spectra but (d) are from the ASD field spectrometer spectral library and scaled using spectral math to match the AVIRIS reflectance scale. (a) Dirty red tile, (b) tile with moss, (c) tile with lichen, (d) AVIRIS pixel of a mixed pixel containing all the endmembers (e) equally weighted average of all clay tile endmembers from the library (f) brown smooth tile (g) oak tree debris on tile (h) dark oxidized tile.

Manufacturers use natural materials such as Hematite, Magnetite and Goethite to color clay tiles (www.monier.com). These iron bearing minerals are used as natural pigments as seen in the VIS region of Figure 24. Several factors contribute to the overall color of the tile but Goethite is typically orange with higher overall reflectivity and Hematite is red (Schwertmann, 1993). Goethite's decrease in the SWIR may be due to contamination (clay and silica). The major difference is seen in the absorption feature centered at approximately 930 nm in Goethite and 880 nm in Hematite. Combinations of these most likely contribute to the various colors of tiles.

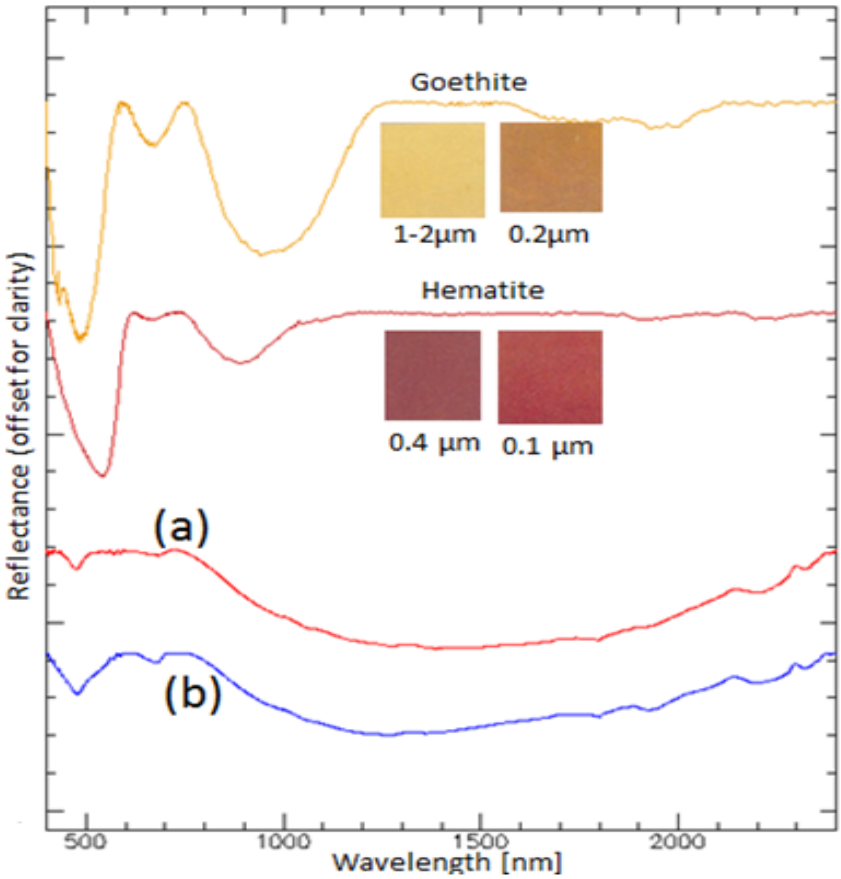

Figure 24. This plot (continuum removed) shows spectra (a) and (b) from Figure 23 with Goethite (FeOOH) and Hematite (Fe_2O_3) from the USGS spectral library of minerals for comparison (Clark, 1993). Samples of Goethite and Hematite colors are given with corresponding crystal size for comparison (From Schwertmann, 1993).

4. Asphalt

Asphalt consists of two parts, a rock (aggregate) and an asphalt mix (hot mix or bitumen). The Strategic Highway Research Program (SHRP) report describes eleven aggregates commonly used: two limestones, two granites, a basalt, a calcareous sandstone, a greywacke, and four gravels from glacial till to cherty conglomerate (Roble et al., 1991). The asphalt mix typically consists of oil, asphaltenes, and resins (Herold, 2007). Figure 25 shows imagery from an assortment of asphalt types found at NPS. Figure 25 shows the increase in reflectance caused by variability in the composition of the asphalt caused by wear, age, or other factors. Features with greater reflectance values have more pronounced spectral features. Materials that are composed primarily of the asphalt mix (i.e., fresh asphalt patches, asphalt sealant) reflect the least but still have the same spectral features. Reflectance of these materials is low and generally increases with longer wavelengths; typical of coals, oil shales, and chars (Herold, 2001).

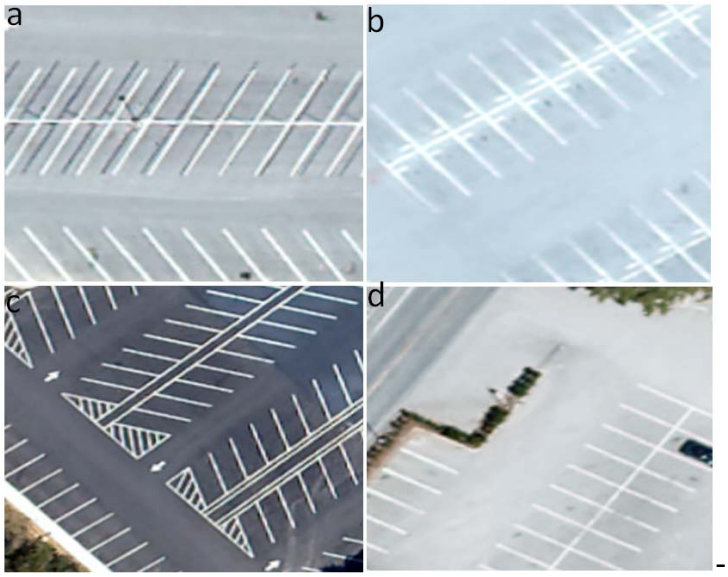

Figure 25. High resolution true color image showing various asphalt types at NPS (white street paint was not seen in AVIRIS endmembers). (a): Older asphalt, smaller loose aggregate with various areas with higher in hydrocarbons either from vehicle traffic or asphalt aging. (b): Parking lot similar to (a) but with a slightly different aggregate size and/or shape affecting the reflectivity. (c): Fresh asphalt sealant causing the darker color. Very minimal aggregate showing through except in high traffic areas. (d): Parking lot showing highest reflectance with a high traffic road surface in the upper left.

Spectral features of asphalt surfaces are primarily due to the type of aggregate and the amount of asphalt mix. Spectra in Figure 26 (AVIRIS and field collected spectra) show the variability in the SWIR region caused by various combinations of asphalt mix and aggregate. AVIRIS derived endmembers are considerably noisier therefore some of these features are difficult to visualize. Those with more asphalt mix and less aggregate show complex spectral features between 2250 and 2300 nm attributable to the hydrocarbons (Herold, 2007). Variability in the depth of the hydrocarbon feature correlates well with asphalt condition caused by either the loss of sealant (top coat) or heavily cracked asphalt (Herold, 2007). Spectrum (f), new asphalt patch, has the deepest absorption feature at 2313 nm. There is less variability in the depth of the hydrocarbon feature in all other spectra. Spectrum (a), which has the least amount of asphalt mix and therefore is the brightest of all spectra collected, shows an increase in reflectance in the NIR region (Figure 27) caused by the spectral response of minerals in the aggregate. The higher reflectivity amplifies spectral features throughout the spectrum. The continuum removed plot (Figure 26) shows an absorption feature in all spectra at 2200 nm most likely caused by clay bearing aggregates.

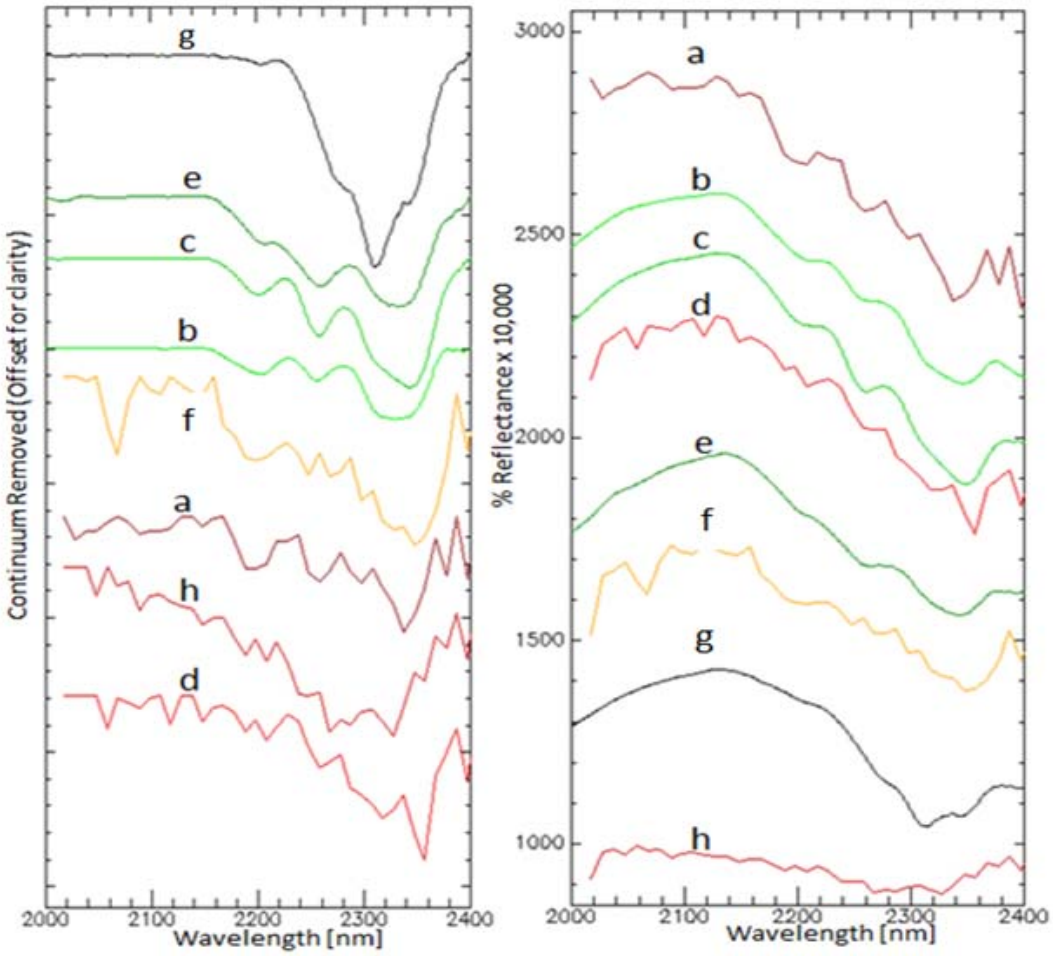

Figure 26. Selected Asphalt spectra from 2000 nm to 2400 nm (AVIRIS and field spectra). Left plot shows continuum removed spectra for analysis of variability associated with depth and shape of spectral features in the SWIR region. Right plot shows percent reflectance for analysis of variability in percent reflectance in the SWIR region. See Figure 26 for specifics.

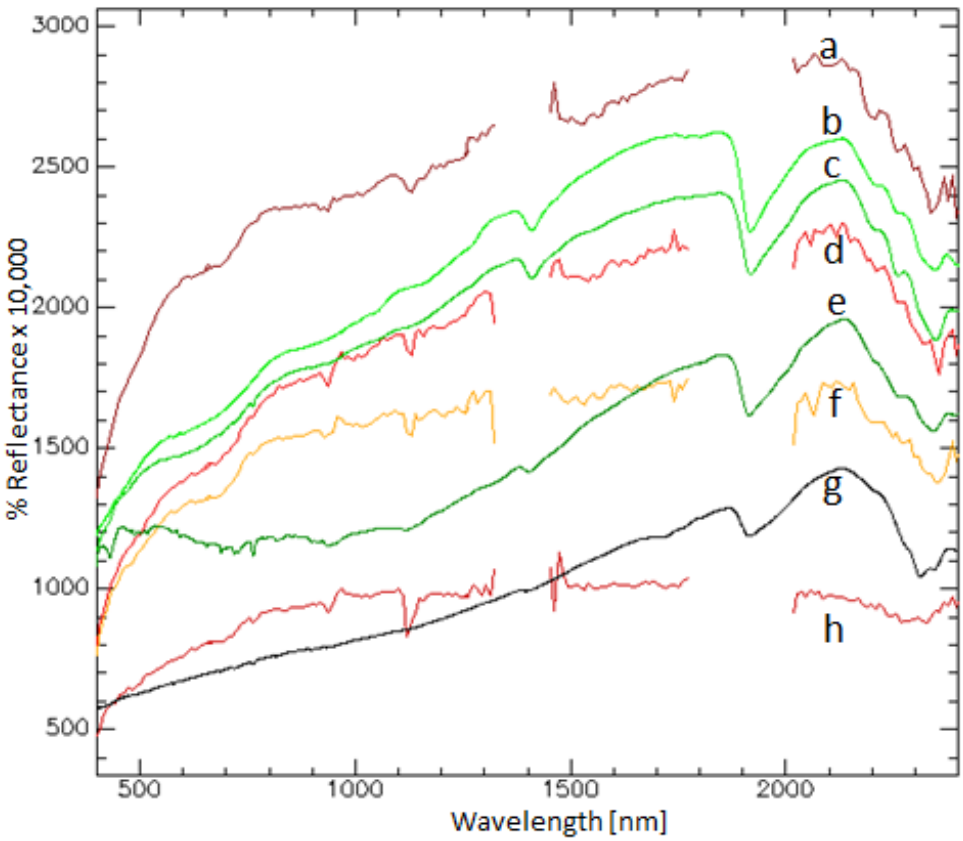

Figure 27. Selected asphalt spectra from AVIRIS and field collections. (a) Fine loose aggregate typical of streets at NPS. (b) slightly worn parking lot surface showing smallest aggregate. (c) Large loose gravel from parking lot. (d) Small loose aggregate from streets. (e) Large loose aggregate from parking lot. (f) Dark top coated blacktop parking lot. (g) New asphalt patch with little or no mineral showing. (h) Fresh sealant on parking lot with minimal aggregate showing. Variability in overall reflectance is attributed to asphalt differences due to wear, age, and other factors.

Intra-class variability in asphalt is mostly due to compositional variability of entrained aggregates, which affects the overall reflectance and depth/position of the absorption bands. Figure 27 shows a variety of asphalt spectra from NPS parking lots as well as an average (red spectrum) of the five spectra used in Figure 25 and 26 for comparison. For the most part, spectral features are preserved throughout all spectra but reflectivity increases with increased aggregate (most likely due to age or wear).

5. Concrete

Visually, concrete seems to be the most variable of all classes on the NPS campus because the color and texture is typically chosen for aesthetics rather than transportation surfaces that are chosen more for their durability (Figure 28). Concrete is composed primarily of rock aggregates, cement (binding agent), and water. Unlike asphalt, concrete is highly reflective and typically darkens with age due to contaminants. Many of the concrete surfaces at NPS are of a highly heterogonous nature representing several materials (i.e., plastic borders, colors of concrete, and brick inlays). The primary use of concrete at NPS is for sidewalks and structural features. Pure pixels are difficult to find using the AVIRIS imagery due to concrete features typically being less than the AVIRIS's 2.3 meter pixels.

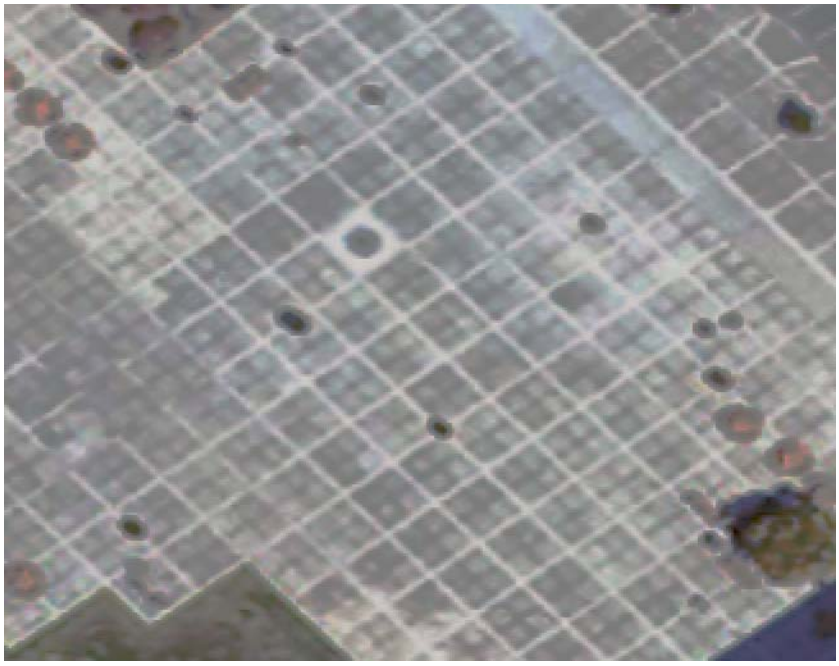

Figure 28. True color high resolution composite image enhanced to emphasize the heterogonous nature of concrete surfaces. Each white-bordered square or block is approximately 8ft x 8ft and is composed of two types of concrete with dark brown plastic borders bisecting the blocks. The feature near the center of the image is a granite circle with concrete border.

Spectra were collected of 62 distinct types of concrete throughout the campus. A subset was created to highlight the spectral variability of select concrete types for further analysis. Newer concrete typically has an overall higher reflectance than older concrete. The lower overall reflectance of older concrete is due to age and contamination with other materials such as soil and vegetation (i.e., algae, moss). Spectrum (a) in Figure 29 is representative of the lighter color concrete from Figure 28. The darker center blocks, (Spectrum d), appear to have the same absorption bands and overall shape yet show an approximately 10% drop in reflectance. Whether this was done on purpose intentionally for aesthetics or not is unknown. The overall shape of all the spectra are generally the same with the exception of (e) and (i), which deviate from the rest of the spectra. Spectrum (i) is of old and worn down concrete contaminated with dirt and debris. A majority of the spectral features remain, yet the spectrum minimum is at 400 nm and reflectance increases into the SWIR where it levels off. Spectrum (h) is also of older concrete but shows a suppressed overall reflectance rather than the steep rise throughout the VNIR into SWIR. Spectrum (e) is of a slick red concrete that is newer. The steep rise in reflectance near 600 nm is due to the red color, then reflectance drops considerably into the SWIR. Spectral features are similar throughout the entire wavelength range.

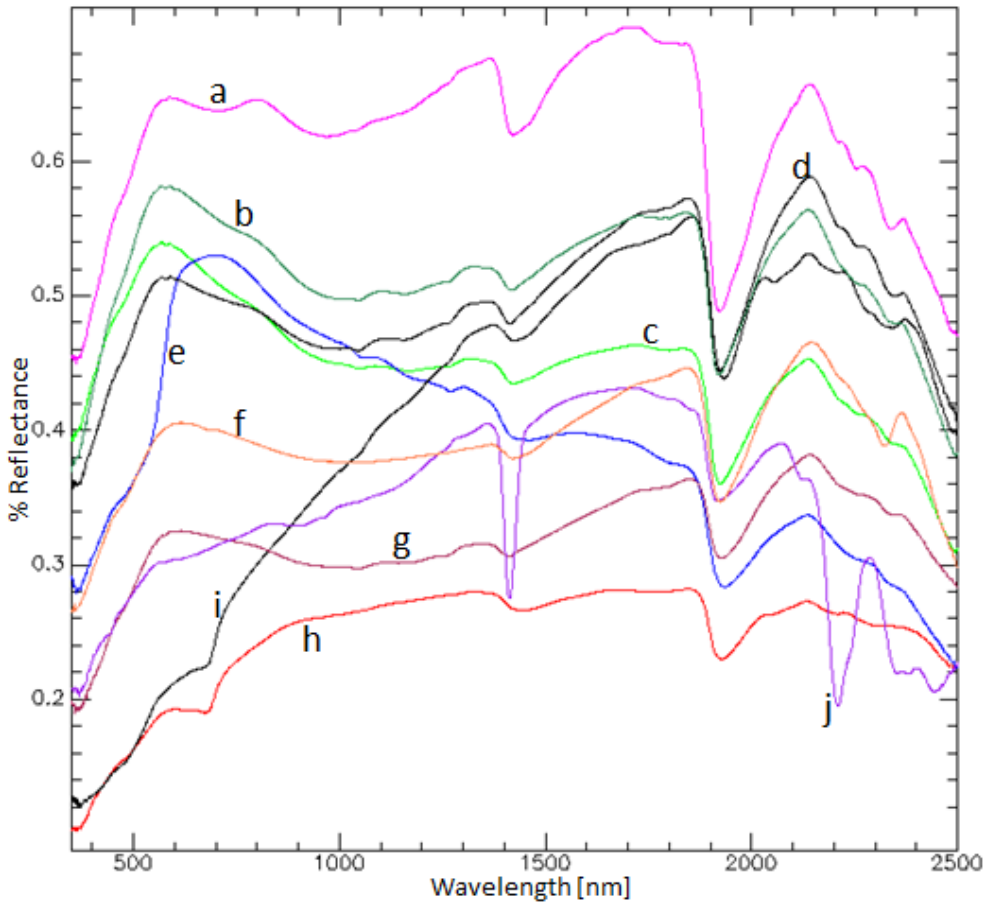

Figure 29. Selection of spectra collected of concrete surfaces. Variability in spectral features and overall reflectance is clearly visible. See text above for specifics.

6. Synthetic Roofs

Synthetic roofs refer to a larger class of thermoplastic roofs typically made of Polyvinyle Chloride (PVC) or Thermoplastic Polyolefin (TPO) (Berdahl et. al., 2008). Specific materials used for NPS synthetic roofs were not investigated any further due to most all synthetic roofs at NPS being made of similar types of synthetic compounds (polymers) that vary mostly due to fouling (i.e., dirt, water puddles, algae growth). Synthetic roofs are installed by overlapping sheets of material, then each sheet is heat welded to produce a waterproof surface. The waterproof property makes this material ideal for flat roofs with low or no foot traffic. Because the roof is waterproof, puddles

collect in discrete portions of the roof that are lower, causing spectral variability due to the water (when present), and the dirt, debris, and minerals that are deposited when the puddles evaporate.

ASD field spectra of synthetic roof materials are shown in Figures 30 and 31. Analysis shows that absorption features are similar throughout all field collected samples of synthetic roof materials but absorption feature depth increases proportionately to percent reflectance. Spectrum (a) and (b) are a good example of this. In Figure 30, spectrum (a) has deep absorpion features (notably broad asymetric absorption features near 1730 nm, 2200 nm and 2300 nm). At the reflectance scale used, these features are not noticable in spectrum (e). Figure 31 (continuum removed) reveals that these features are actually present in Spectrum (e), but much shallower, probably because of contamination (obscuration) of the principal roof material. The overal decrease in reflectance illustrated by Spectrum (e) may affect the ability to classify pixels with heavily soiled materials.

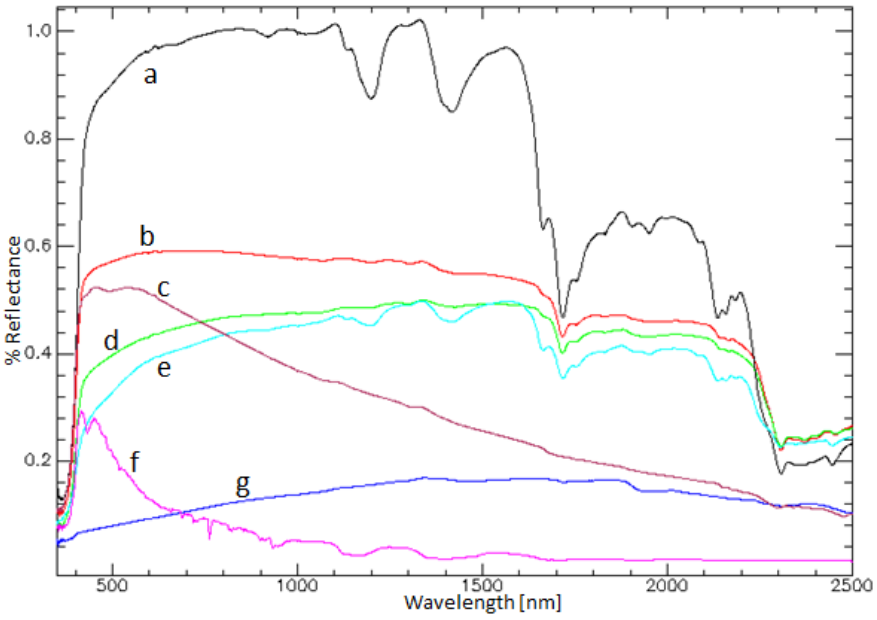

Figure 30. Variability in synthetic white roof surfaces from Root Hall ("A" on Figure 21). (a): Rough synthetic surface. (b): Clean smooth synthetic surface. (c): Grey painted metal on air conditioner unit. (d): Soiled surface with various dirt and debris. (e) gray surface of similar material used for walkway. (f): Grey paint on metal air conditioner. (g): Heavily soiled surface.

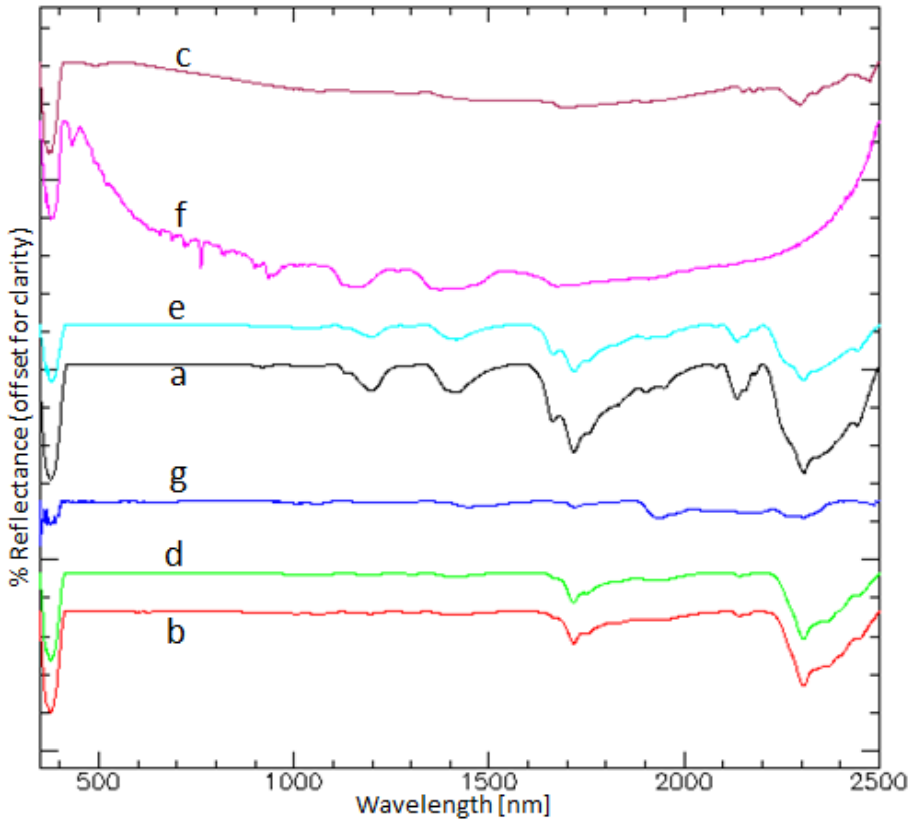

Figure 31. Continuum removed stacked spectra from Figure 31 for analysis of absorption features. (a): rough surface. (b): clean smooth surface. (c): soiled surface with various dirt and debris. (d): gray surface of similar material used for walkway. (e): heavily soiled surface.

7. Painted Surfaces

Paint is used in the urban environment for many purposes. Road paint occurs in many colors, painted concrete is used for aesthetic purposes, tennis and other sporting surfaces are typically painted, and all cars are painted. This is a unique problem in that classification of a land use cannot necessarily be classified by the paint that is used. Concrete, asphalt, and roofing materials all have spectral characteristics that are unique to that material and that material is most likely specific to the application. Once a surface is painted, however, almost all spectral features of the underlying material are lost, therefore the ability to classify the building material is lost.

Figure 32 is a continuum removed stacked plot representing a variety of spectra collected with the ASD field spectroradiometer for painted surfaces. Absorption features

(notably the one near 2270 nm) occur in all spectra. The majority of the spectral separability lies within the VIS region, corresponding to the color of the paint (reflectance peak corresponding to paint color). White and grey paint are featureless in the VIS but are distinguishable by their relatively high reflectance.

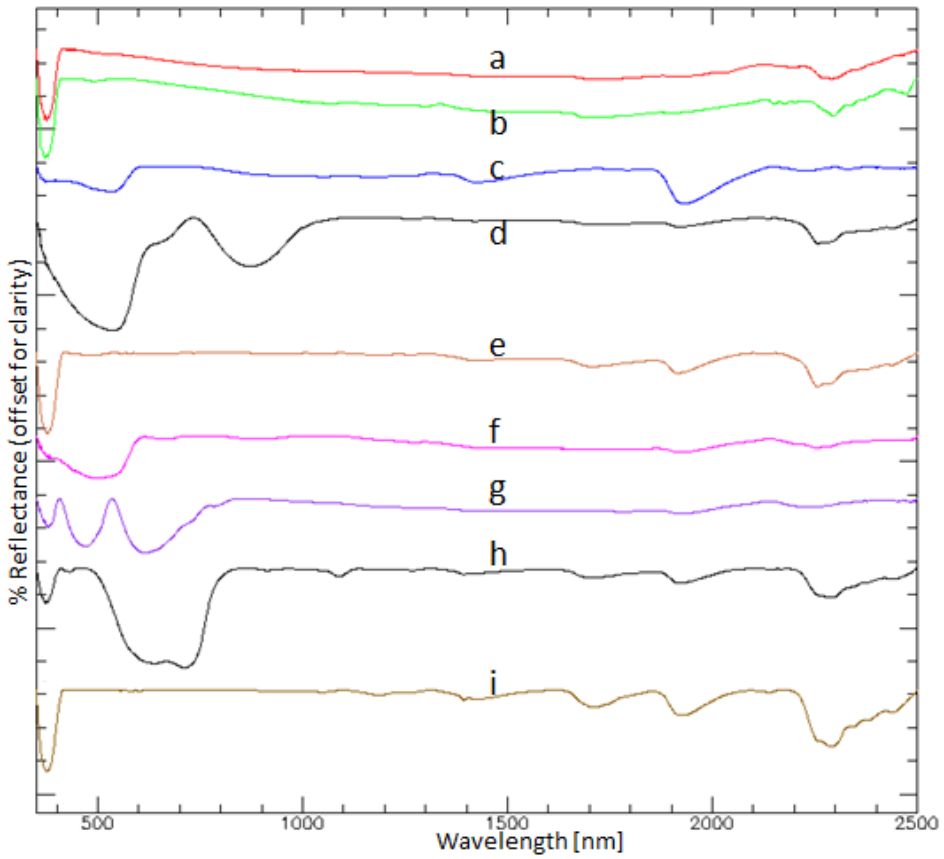

Figure 32. Continuum removed plot of painted surfaces. Variability is mostly in the VIS region due to the color of the paint. Absorption features in the SWIR are consistent but variable with overall reflectance of spectra. (a) grey paint with non-slip rough surface used on the walking surfaces of Spanagel Hall's roof; (b) grey paint used for air conditioner units; (c) red concrete, possibly paint or other additive for color; (d) tennis court newer red paint; (e) white line from tennis court; (f) tennis court older red paint; (g) tennis court green paint; (h) blue street paint; (i) white street paint

8. Spectral Variability of AVIRIS Data Using Spectral Angle Mapper

The urban masked areas were analyzed using classification of the AVIRIS data with image endmember spectra and the SAM algorithm as previously described in the Methods section. AVIRIS image classes are representative of inter-class variability because endmembers were chosen from each class of material (i.e., specific building roofs or transportation surfaces). SAM was found to be decent at classification of larger classes such as all the synthetic roofs with minimal false positives but is not an ideal classifier for mapping sub-pixel data due to the inability for SAM to deal with mixed pixels.

The SAM algorithm is used in this thesis as a measure of spectral variability between endmembers of classes that are distinguishable using 2.3 meter AVIRIS HSI. Spectra were sampled from pure pixels, then spectral angles for classification were determined subjectively to map the occurrence of the material taking into account the spectral variability of other materials in the study area. More variable classes will require an inherently smaller spectral angle to produce spatially coherent classification maps corresponding to the selected endmember. Less variable classes can be mapped using a larger spectral angle because of their homogeneity and lack of spectral mixing. Del Monte Lake has few other spectrally similar materials within NPS, and thus was mapped as a single homogeneous class using a relatively large spectral angle of 0.4 radians in the SAM algorithm. A larger spectral angle of 0.6 radians was used to determine materials that could be confused with lake water (Figure 33).

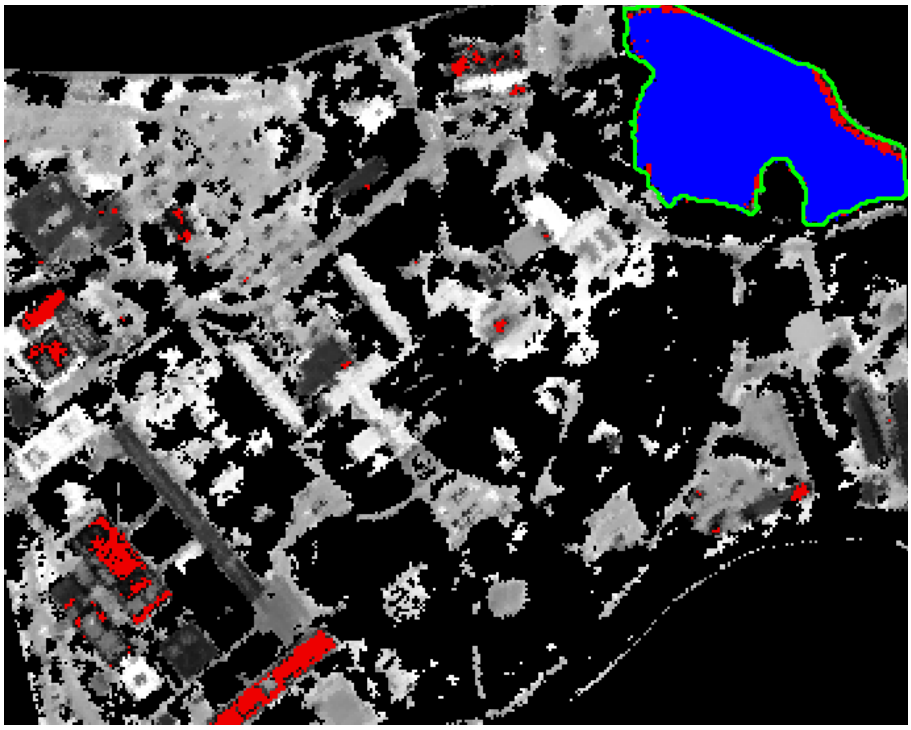

Figure 33. AVIRIS SAM rule image. Darker areas correspond to smaller angles between the reference spectrum and test (image) spectrum. A threshold of 0.4 (red) is used to classify lake pixels (36,293 m^2) without classifying other pixels. Using a threshold of 0.6 shows pixels with spectra that may be confused as water when they are not actually water (36,293 m^2).

Clay roofing tiles were divided into classes specific to the building to which they belonged. Previous spectroscopic analysis of field spectra and AVIRIS pixels show that there may be enough spectral variability between various building roofs to allow each building, or class of building, to have a separate class. Visually, each roofing material looks unique due to the overall color of the tiles, but the spectral variability high enough that it is difficult to map each building without also mapping pixels that correspond to other buildings. Almost all of the tile roof classifications only over-classified pixels corresponding to other clay tile or red gravel roofs, with the exception of a few asphalt pixels.

Figure 34a is a classification of the NPS Fitness Center red tile roof. The tiles are relatively homogeneous, with low spectral variability. The actual roof is approximately

1,054 m^2 and the classification using a 0.6 threshold is 1,393 m^2. Almost all of the Fitness Center pixels are classified, and over-classification is limited to a few pixels from various other clay tile roofs.

Figure 34b is of the main building of Hermann Hall. Roof area is 3,375 m^2 and classification at 0.6 radians classifies 4,262 m^2. The tiles are of various colors, and noticeably darker than the tiles used for the Hermann Hall wings. The roof is mostly homogenous but the complicated geometry of the roof may cause mixed pixels if the image is not taken at nadir. The tiles are almost spectrally identical to the tiles used for the Quarters, which explains why the Quarters are classified with Hermann Hall endmembers.

Herman Hall's wings (Figure 34c) are even more geometrically complicated than the main building and have a similar tile, yet slightly lighter in color. The two wings cover 3,000 m^2 and the classification at 0.6 radians resulted in 3,847 m^2 classified. Most pixels over-classified were of the main building, a few of the Quarters, some bare dirt, and some asphalt pixels.

The endmembers used for the Quarters clay tile roof (Figure 34d) were most likely not pure pixels, therefore classification exhibits some confusion due to spectral mixing. The roofs cover approximately 1,774 m^2 and the classification at 0.60 radians covers 4,429 m^2. The low spectral variability between the main building of Hermann Hall and the Quarters resulted in most of Hermann Hall tiles being classified as Quarters. Hermann Hall clay tiles were also over-classified when using the endmembers for the quarters. Various other clay tile roofs were over-classified as well.

Figure 34e is of a portion of the libraries roof that is covered with coarse red gravel. The red gravel covers approximately 1,872 m^2 and the classified pixels cover 1,146 m^2 at a 0.6 radians threshold. Other red gravel roofs were also classified at this threshold but the red gravel is mostly spectrally unique to the library with only a few over-classified pixels.

The red gravel used on Ingersoll Hall is slightly different than other red gravel roofs and is spectrally similar to clay tile roofs. The roof is entirely red gravel with

various air conditioner units and other materials near the center. The entire roof covers 2,367 m^2 and the classified pixels cover 4,014 m^2. Various clay tiles from Hermann Hall and portions of all the red gravel roofs were misclassified.

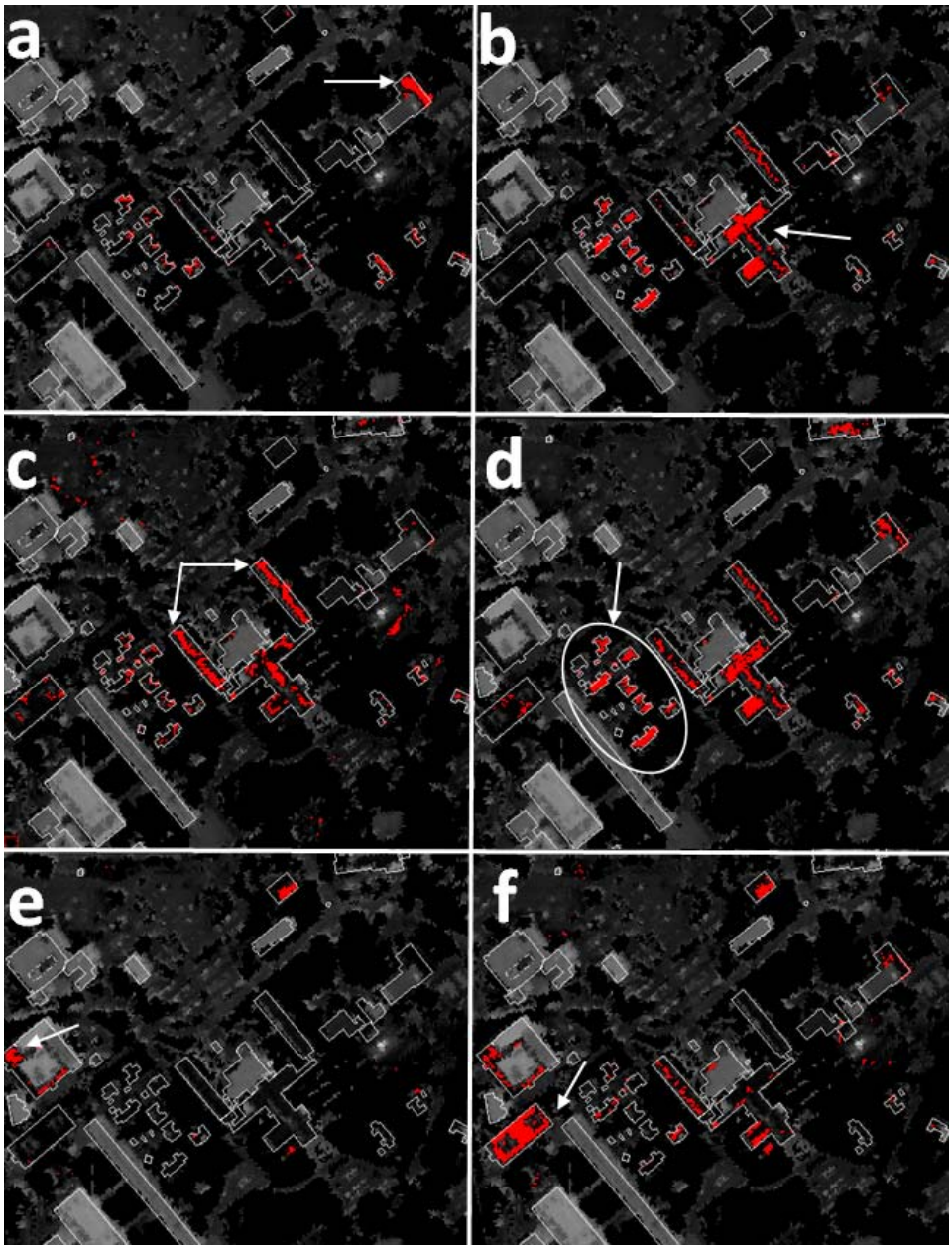

Figure 34. AVIRIS SAM rule images of clay tile and red roofing gravel classes. A spectral angle of 0.60 was used as a threshold for all images. Arrows point to the building that is being classified. (a) Fitness Center red tile; (b) Hermann Hall main building red tile; (c) Hermann Hall wings red tile; (d) Quarters red tile; (e) Library red gravel; (f) Ingersoll Hall red gravel.

Table 6 shows the results for the materials used in Figure 36 ranked according to decreasing spectral variability calculated by dividing the SAM classified area by the actual area for each endmember. A lower index (higher rank) should indicate lower spectral variability. A 0.60 spectral angle was chosen as a standard threshold, therefore the materials were over-classified and under-classified with the quarters (2.49 index) being the most over-classified and the library red gravel (0.60 index) being the most under-classified.

Name	Classified Area	Actual Area	Index	Rank
Quarters Red Tile	4429	1774	2.49	1
Ingersoll Red Gravel	4014	2367	1.69	2
Fitness Center Red Tile	1393	1054	1.32	3
Hermann Hall Wing Red Tile	3847	3000	1.28	4
Hermann Hall Main Bldg Red Tile	4262	3375	1.26	5
Library Red Gravel	1146	1872	0.61	6

Table 6. Variability or separability index based on area classified divided by actual area of material.

9. Asphalt Roads

Asphalt was classified in Figure 35 as one class using the SAM algorithm with a threshold of 0.12 radians (red) and 0.04 radians (green). Analysis was performed to determine inter-class variability to better understand what non-transportation surfaces could be confused as asphalt roads. Figure 35 shows several examples of non-transportation surfaces being confused as asphalt roads. Given a spectral angle large enough to classify a majority of the asphalt surfaces (0.12 radians, red on Figure 35), many non-transportation surfaces are also classified as asphalt roads. The lowest spectral angle that classifies only asphalt roads is approximately 0.04 radians (green on Figure 35). Figure 35 "**a**" is a rooftop made of a grey concrete, that closely resembles a lighter color asphalt surface. Figure 35 "**b**" shows various pedestrian sidewalks and paving stones classified as asphalt. Figure 35 "**c**" shows bare earth classified as asphalt. Figure 35 "**d**" shows a baseball diamond classified as asphalt.

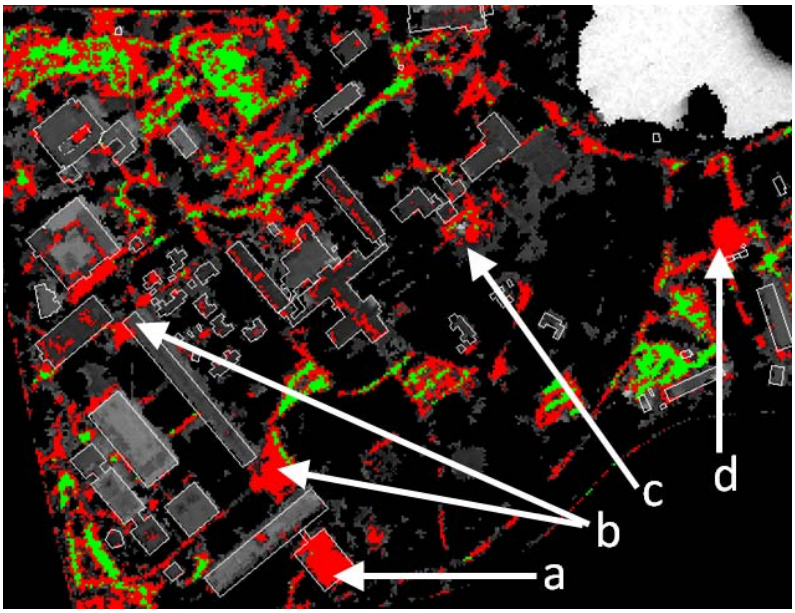

Figure 35. Composite image of all the classes classified using the SAM algorithm and spectral angles subjectively selected to minimize over- or under-classification of the known material (asphalt). (a) King Hall gray concrete roof; (b) concrete pedestrian paths; (c) bare earth; (d) baseball diamond

10. Synthetic Roofs

Most flat roofs at NPS that do not allow public access have some type of synthetic covering. Some have red gravel. Figure 36 shows that the synthetic roofing materials are relatively spectrally unique, with very few pixels classified outside of areas expected to have these materials. The grey paint and/or another surface on Spanagel Hall (Figure 36 "a") were also classified as synthetic roof using a spectral angle of 0.12 radians. Materials used for almost all the NPS synthetic roof coverings are spectrally similar, with the exception of the synthetic roofing material used for the Navy Exchange building (Figure 36 "b"). Buildings that seem under-classified have other features on the roof (i.e., solar panels, air conditioner units, skylights, etc.) that affect the classification.

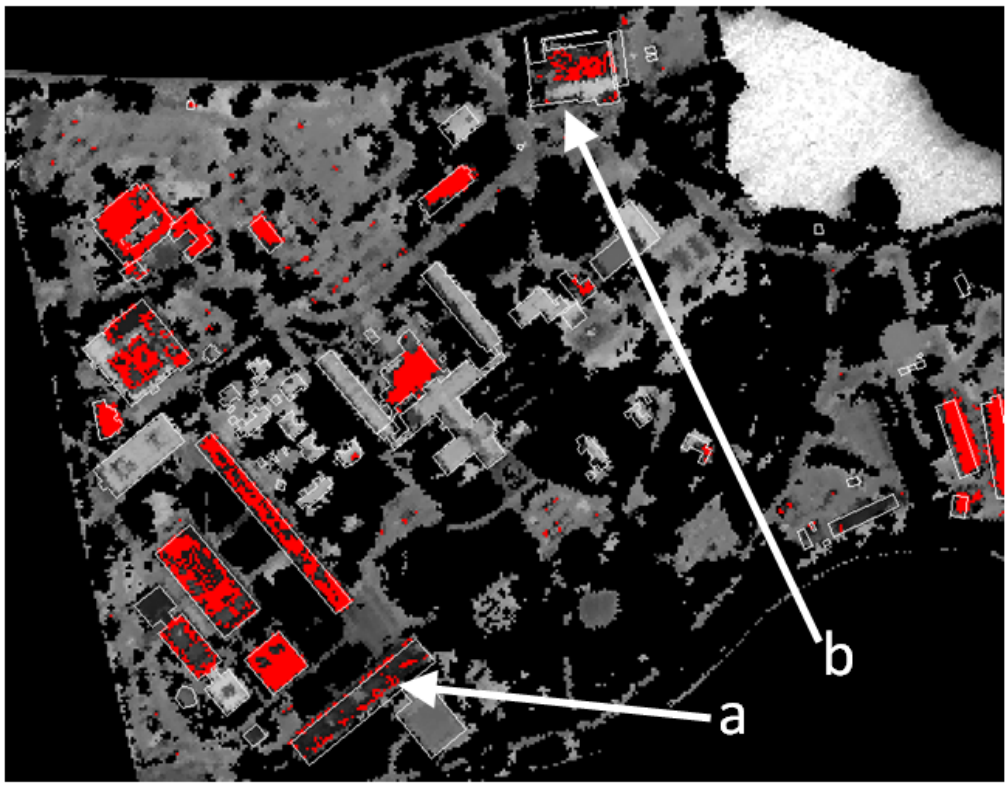

Figure 36. Synthetic roof classification using an AVIRIS SAM spectral angle of 0.12 radians. (a) Spanagel Hall grey painted roof; (b) Navy Exchange grey synthetic roof

11. Spectral Angle Mapper for Classification

As previously stated, the SAM algorithm is not ideal for classification of urban areas due to a majority of pixels in the urban area having mixed pixels. Figure 37a shows an AVIRIS SAM classification map that gives a general idea of the spatial distribution of the materials used for this spectral variability analysis using a spectral angle selected to minimize over- or under-classification based on best match to known materials' distributions. Post-classification sieving and clumping of pixels was performed for aesthetic purposes to aid in interpretation. The material name used for classification is provided in the key with corresponding spectra plotted below the classification image in Figure 37b.

Synthetic roofs seem spectrally similar when using the SAM classifier. By using a lower threshold, it is possible to identify materials that match the spectral signature of the

endmember used for classification but if all synthetic roofs need to be classified using a non-specific endmember then a higher threshold could be used without very much over-classification of other non-synthetic roofing materials. This ability makes the SAM classifier robust to using an endmember that represents one synthetic roof without losing the ability to classify all synthetic roofs. As a target detector, the SAM classifier may be able to find areas containing synthetic roofs then narrow the search to a more specific material using an endmember more specific to the target and decreasing the threshold. MTMF classification is discussed later and would be a well suited to find specific materials once all synthetic roofs are detected with the SAM classifier.

Concrete was hypothesized as difficult to classify with a classifier that does not take into account spectral mixing. This proved true in the SAM classification performed in this study, with decent performance only in areas that lack spectral mixing. Sidewalks and concrete features are an important aspect of the urban environment, therefore the inability to classify subpixel concrete features is a major drawback of using SAM for urban remote sensing. In areas where spectral mixing was not much of an issue, spectral variability between concrete and other materials was high enough to detect a majority of the concrete areas without over-classification of other materials.

It is difficult to analyze asphalt spectral variability due to the dynamic nature of parking lots and other transportation surfaces. In the SAM classification, it is possible to more or less determine where roads and parking lots are located, but since the vehicle traffic and/or various road paint continually affects the spectral mixing of the surface, it is difficult to make conclusions on the performance. Over-classification seems to be limited to King Hall (roof material undetermined) while using a threshold that includes a majority of the asphalt surfaces.

Clay roofing tiles were treated as several classes to determine if inter-class variability could be determined from image derived endmembers, therefore the thresholds are generally lower to account for low variability between various clay tile types. Larger building roofs such as Hermann Hall are more suited for SAM classification due to a spectral mixing of pixels representing the smaller roofs (quarters roofs). There is some

confusion between concrete and the main Hermann Hall roof, but portions of other red tile roofs are not classified with the threshold used.

Solar panels are spectrally unique, therefore a higher threshold can be used to classify all solar panels with very little confusion with other materials. Not much information is available for the type of solar panels used, but visual inspection suggests that there is very little variability between the types of solar panels used on various roofs.

Spanagel Hall has a highly heterogonous roof containing various antennas and air conditioner units which would seem to cause spectral mixing and under-classification of the predominant grey painted concrete found on the roof. While using a relatively high threshold, it is possible to classify a majority of Spanagel Hall without classifying other grey paints commonly found on campus.

There are two sets of tennis courts found on campus and only the newer of the two was classifiable with SAM. The older tennis court is bounded by heavy vegetation and there are typically pine needles on the court due to the court not being used on a regular basis. A majority of the pixels representing the newer court were classified with the outer pixels (red paint) being unclassified most likely due to spectral mixing with other surfaces.

The baseball diamond is over-classified using SAM at a relatively low threshold with other materials such as clay tile roofs and red gravel being confused with baseball diamond. The material used for the baseball diamond is relatively homogenous but all pixels are not classified with the endmember used.

Relatively small portions of roofs contain red gravel (i.e., library roof) and those areas are cluttered with other features causing spectral mixing. Portions of the red gravel were partially classified, but under-classification is most likely due to spectral mixing with other roof features.

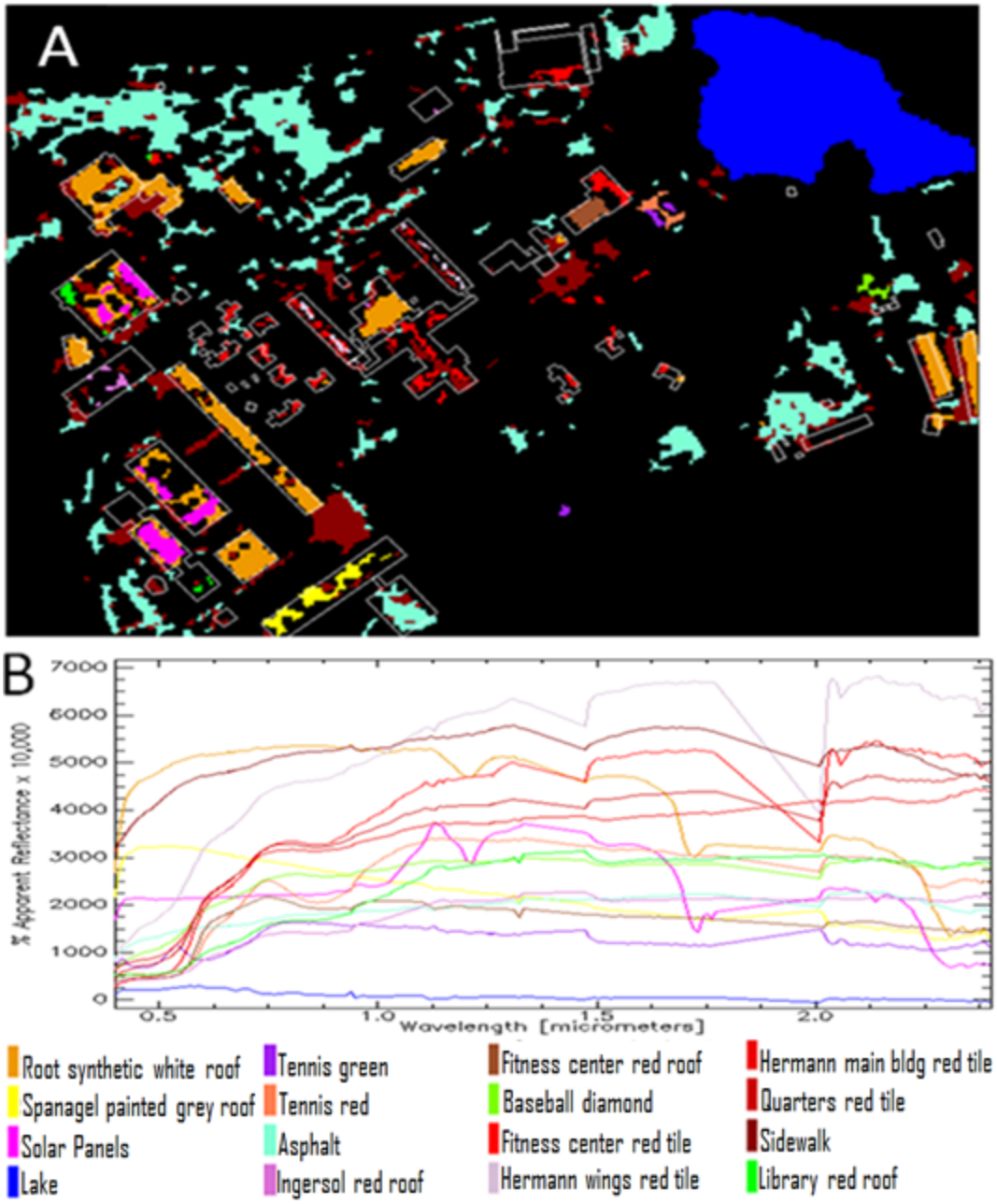

Figure 37. (A) Spectral Angle Mapper (SAM) classification of the AVIRIS data using image derived endmembers. Pixels were clumped and sieved to better visualize the data. (B) Endmember spectra are plotted below in Figure 37B with corresponding color scheme.

12. Mixture Tuned Match Filtering Classification

The MTMF classification algorithm is better suited for sub-pixel analysis due to the ability to select pixels with both a high infeasibility score and an MF score above the background distribution. As discussed in the methods section, the false positives are decreased by plotting MF and infeasibility on a 2-D scatter plot then selecting a proper threshold that best classifies the material.

Selecting a strict upper bound for MF and a lower bound for infeasibility is a less subjective method of classifying pixels, but over- and under-classification was common. It was found that most materials had a natural grouping in the high infeasibility and low MF region therefore pixels were manually selected from the grouping to account for this.

Asphalt was difficult to classify with the MTMF due to over-classification occurring in areas of concrete. The classification used in Figure 38 is a compromise between under-classification of asphalt and over-classification in areas of concrete. This is a good example of how classification is affected by spectral variability. Synthetic roofs were found to be more sensitive to under-classification if the endmember used does not represent a certain synthetic material. Visually, all synthetic roofs seem spectrally similar but two synthetic roofs (along eastern boundary in Figure 38) were not classified. In the 2-D scatter plot, these roofs were represented by a distinct grouping that indicates they are made of a different material than all the other NPS synthetic roofs. This points out the sensitivity of the MTMF to classify specific materials represented by the measured endmember.

Red tile roofs were divided into various classes representative of the building, therefore classification success using MTMF varies from other materials classified. Almost all pixels representing the quarters roofs were classified with very little over-classification. The Hermann Hall wings were slightly under-classified along the roof edges with very little confusion with other tile types. Hermann Hall's main building is under-classified in regions with complex geometries such as the bell tower. Other types of red tile and red gravel roofs were classified with similar success. By using a unique

endmember for each clay tile roof, it is possible to use the spectral variability inherent to clay tile roofs to differentiate roofs of various buildings.

Classification of other materials with a smaller spatial extents demonstrated classification success similar to the roofing materials. A majority of the tennis courts red and green materials are classified within the newer court. The green paint on the older court is also classified, indicating that either the red material is obstructed by fallen vegetation, or a different red material was used for the older tennis court. A majority of the baseball diamond's pixels were classified with little or no over-classification. All pixels representing solar panels on roof tops were classified. The grey paint used for Spanagel Hall's roof was detected on Spanagel Hall but a majority of the pixels are under-classified.

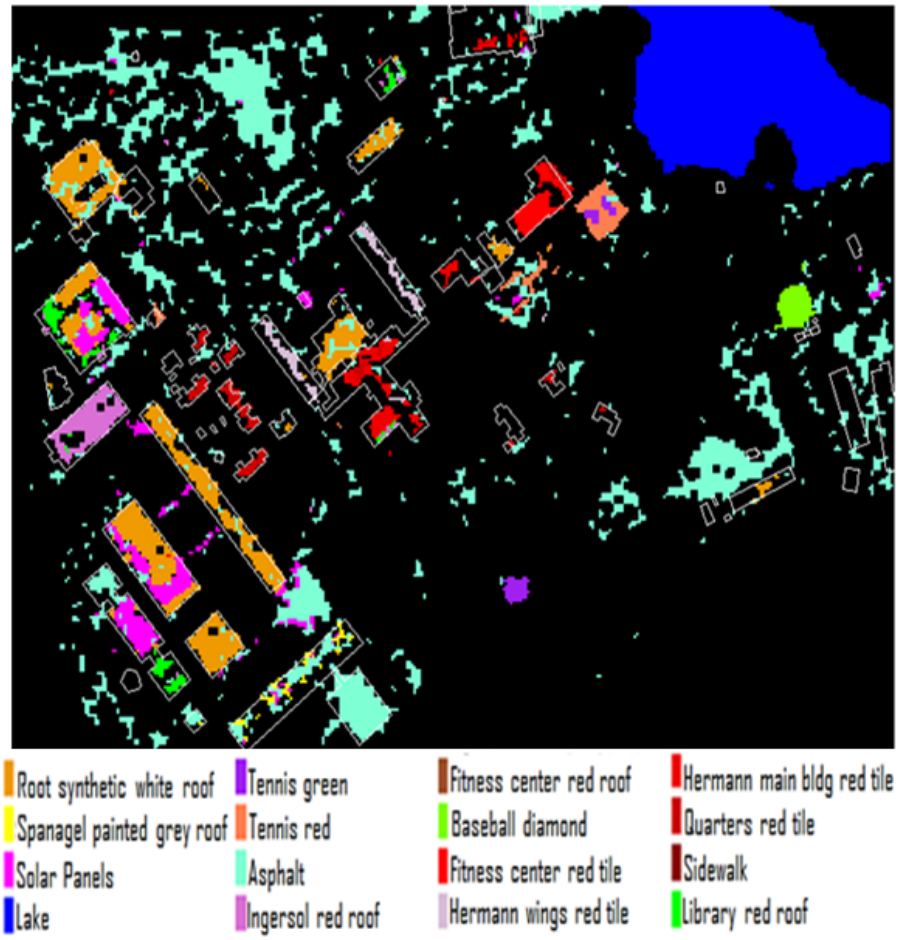

Figure 38. Mixture Tuned Match Filter classification image. Endmember spectra are shown in Figure 37b with the same color scheme.

THIS PAGE INTENTIONALLY LEFT BLANK

V. CONCLUSIONS AND FUTURE WORK

A. CONCLUSIONS

This thesis provides a look into the complex nature of urban materials and their intra- and inter-class variability. A spectral library was created using a field spectroradiometer to assess variability between spectra of selected urban materials. Endmembers were derived from AVIRIS hyperspectral imagery to assess inter-class variability and to describe intra-class variability using two common classification algorithms (MTMF and SAM). A qualitative analysis of selected spectra was performed to determine the composition of each material and to determine where spectral variability is greatest for each material. Library spectra were compared to AVIRIS spectra to determine how intra-class variability contributes to spectra from hyperspectral imagery.

Visual analysis of the spectra collected in the field provided insight into the intra-class variability caused by the various components of a material. This dataset was found to be too specific to a single material to be useful for a classification map (inter-class) covering the entire campus. A larger field-of-view was created synthetically by averaging the spectra of all the materials within a pixel, but it was found that image-derived endmembers were superior for investigating inter-class variability. The research also demonstrated that materials generally increase or decrease in overall reflectance as a function of wear or age with small changes in spectral features caused by fouling or other factors.

Almost all major classes of urban materials reviewed in this study have a high enough inter-class spectral variability to allow discrimination between various classes when using common classification algorithms, but the results show that one classification method is not suitable for all applications. This study is specific to the small spatial extent of the Naval Postgraduate School. It is expected, however, that if the same study was performed on a larger dataset, materials with similar spectra would cause more spectral confusion and over-classification. For the NPS site, classification of a specific land use (i.e., transportation, roofing, recreational) was difficult because similar building materials

or paint are used for various purposes. Asphalt roads were also difficult to classify as a land use class because the materials used in these roads (asphalt and aggregate) are used for a variety of applications in the urban setting. Asphalt also exhibited high intra-class spectral variability (principally due to aggregate type and amount); therefore the abundance of asphalt may be under-classified. Concrete was found to have high intra-class variability in the VIS region due to the color added for aesthetic reasons. This, along with high spectral mixing, makes concrete difficult to classify with the both SAM and MTMF. Synthetic roofs were treated as a single class and appear to be a single class with low intra-class spectral variability when classified with SAM. There were several synthetic roofs that were not classified with MTMF due to inter-class variability and a lack of endmembers representing other synthetic roof types. Several types of painted surfaces found throughout the NPS campus caused spectral confusion because of the many types of surfaces painted with similar paint.

This research demonstrates the spectral variability of urban materials and the effect the variability has in choosing a suitable classifying algorithm to map either intra- or inter-class variability. MTMF performs much better than SAM in finding either materials with low intra-class spectral variability or for classification of materials that are well documented in a spectral library. If the purpose is to classify using only the inter-class variability and a non-specific endmember, then SAM is much better suited because of the ability to subjectively tune the threshold to span a large class of materials that has high spectral variability.

B. FUTURE WORK

There is still much work to be done in urban spectral remote sensing. Although the field spectra collected were ideal for examining the components of a material, they are not ideal for classification purposes. This research would benefit by increasing the spectral library to contain more field spectra from classes that were found to have relatively high spectral variability (i.e., synthetic roofs). Improved direct access to areas, such as most of the clay tile roofs, would allow spectra to be collected with a larger field-of-view foreoptic on the field spectroradiometer. Field spectra taken with a large field-of-

view foreoptic would better approximate a typical AVIRIS pixel for a given class, therefore improving the classification and decreasing any artificial variability caused by spectral mixing when extracting endmembers from images.

A better method of organizing spectra along with metadata would benefit anyone else using these data for research. Current spectral libraries include metadata in additional text files but information such as where the spectra were collected (coordinates), post-processing methods, and detailed descriptions of the material are typically not included with the data. Pictures of each material would have aided in the identification of minerals in some of the spectra collected in the field. A small camera mounted on the foreoptic that takes time lapse pictures or video could be used to correlate with the spectra by including an accurate time stamp in the picture file.

The Naval Postgraduate School is roughly 50% vegetation, making it ideal for studying the spectral variability of vegetation. Data fusion techniques with LiDAR would allow the delineation of buildings from ground and further decrease false positives when doing classification. Spectral variability is subject to the classifier used; therefore better results may be possible using a variety of classifiers for various materials, depending on the materials spatial extent and the spectral variability. A machine learning algorithm might be beneficial to selecting natural groupings of spectra when using the MTMF algorithm rather than manually selecting what pixels belong to a material. A machine learning algorithm would also be able to group pixels in the image that correspond to building roofs or transportation materials based on their expected shape or size.

THIS PAGE INTENTIONALLY LEFT BLANK

LIST OF REFERENCES

Agar, B., & Coulter, D. (2007). Remote sensing for mineral exploration—A decade perspective 1997–2007. *Proceedings of Exploration 07: Fifth Decennial International Conference on Mineral Exploration*, 109–136.

Anderson, J. R., Hardy, E. E., Roach, J. T., & Witmer, R. E. (1976). A land use and land cover classification system for use with remote sensor data. *Geological Survey*, *671*, 1–41.

Berdahl, P., Akbari, H., Levinson, R., & Miller, W. A. (2008). Weathering of roofing materials–an overview. *Construction and Building Materials*, *22*(4), 423–433.

Boardman, J. W., & Kruse, F. A. (2011). Analysis of imaging spectrometer data using N-Dimensional geometry and a mixture-tuned matched match filtering (MTMF) approach. *Transactions on Geoscience and Remote Sensing (TGARS), Special Issue on Spectral Unmixing of Remotely Sensing Data*, *49*, 4138–4152

Clark, R. N., Swayze, G. A., Gallagher, A. J., King, T. V. V., & Calvin, W. M. (1993). The U.S. Geological Survey, Digital Spectral Library: Version 1: 0.2 to 3.0 microns, U.S. Geological Survey Open File Report 93–592.

Gao, B., & Goetz, A. H. (1990). Column atmospheric water vapor and vegetation liquid water retrievals from airborne imaging spectrometer data. *Journal of Geophysical Research*, *95*(D4), 3549–3564

Grove, C. I., Hook, S. J., & Paylor, E. D. (1992). Laboratory reflectance spectra for 160 minerals 0.4–2.5 micrometers: *JPL Publication* 92–2

Goetz, A. F. (2009). Three decades of hyperspectral remote sensing of the Earth: A personal view. *Remote Sensing of Environment*, *113*, S5-S16.

Goetz, A. F., Vane, G., Solomon, J. E., & Rock, B. N. (1985). Imaging spectrometry for earth remote sensing. *Science*, *228*(4704), 1147–1153.

Heiden, U., Roessner, S., Segl, K., & Kaufmann, H. (2001). Analysis of spectral signatures of urban surfaces for their identification using hyperspectral HyMap data. In *Remote Sensing and Data Fusion over Urban Areas, IEEE/ISPRS Joint Workshop 2001*, 173–177

Herold, M., Schiefer, S., Hostert, P., & Roberts, D. A. (2006). Applying imaging spectrometry in urban areas. *Urban Remote Sensing*, 137–161.

Herold, M. (2004). Spectrometry for urban area remote sensing—Development and analysis of a spectral library from 350 to 2400 nm. *Remote Sensing of Environment*, *91*(3–4), 304–319.

Herold, M., Gardner, M., & Roberts, D. (2003). Spectral resolution requirements for mapping urban areas. *IEEE Transactions on Geoscience and Remote Sensing*, *41*(9), 1907–1919.

Herold, M. (2007) Spectral Characteristics of Asphalt Road Surfaces. *Remote Sensing of Impervious Surfaces*, 237–247

Kramer, H. J. (2002). *Observation of the Earth and its Environment: Survey of Missions and Sensors*. Gilching: Springer Verlag.

Kruse, F. A., Clasen, C. C., Kim, A. M., & Carlisle, S. C. (2012) Effects of spatial and spectral resolution on remote sensing for disaster response: Proceedings of the IEEE Geoscience and Remote Sensing Symposium (IGARSS 2012), 22–27 July 2012, Munich, Germany.

Kruse, F. A., Lefkoff, A. B., Boardman, J. W., Heidebrecht, K. B., Shapiro, A. T., Barloon, P. J., & Goetz, A. F. H. (1993). The spectral image processing system (SIPS)—interactive visualization and analysis of imaging spectrometer data. *Remote Sensing of Environment*, *44*(2), 145–163.

Kruse, F. A., Boardman, J. W., Huntington, J. F., Mason, P., & Quigley, M. A. (2002). Evaluation and validation of EO-1 Hyperion for geologic mapping. In *Geoscience and Remote Sensing Symposium, 2002. IGARSS'02. 2002 IEEE International*, Vol. 1, 593–595

McCoy, R. M. (2004). *Field methods in remote sensing*. New York: Guilford Press.

Nasarudin, N. E. M., & Shafri, H. Z. M. (2011). Development and Utilization of Urban Spectral Library for Remote Sensing of Urban Environment. *Journal of Urban and Environmental Engineering (JUEE)*, *5*(1), 44–56.

Olsen, R. C. (2007). *Remote sensing from air and space* (Vol. 162). Bellingham: Society of Photo Optical.

Price, J. C. (1997). Spectral band selection for visible-near infrared remote sensing: spectral-spatial resolution tradeoffs. *Geoscience and Remote Sensing, IEEE Transactions on*, *35*(5), 1277–1285.

Powell, R. L., Roberts, D. A., Dennison, P. E., & Hess, L. L. (2007). Sub-pixel mapping of urban land cover using multiple endmember spectral mixture analysis: Manaus, Brazil. *Remote Sensing of Environment*, *106*(2), 253–267.

Richards, J. A. (1999). *Remote sensing digital image analysis: an introduction*. Canberra: Springer.

Robl, T. L., Milburn, D., Thomas, G., Groppo, J., O'Hara, K., & Haak, A. (1991). *The SHRP materials reference library aggregates: chemical, mineralogical, and sorption analyses*. Washington, DC: Strategic Highway Research Program.

Roberts, D. A., & Herold, M. (2004). Imaging spectrometry of urban materials .*Infrared Spectroscopy in Geochemistry, Exploration and Remote Sensing, Mineral Association of Canada, Short Course Series*, *33*, 155–181.

Rowan, L., & Abbott, E. (1987). Analysis of shuttle multispectral infrared radiometer measurements of the Western Saudi-Arabian shield. *Geophysics*, *52*(7), 907–923.

Schwertmann, U. (1993). Relations between iron oxides, soil color, and soil formation. *Soil Color*, (soil color), 51–69.

Sellers, J. J., Astore, W. J., Giffen, R. B., Larson, W. J., Kirkpatrick, D. H., & Shute, A. (2005). *Understanding Space: An Introduction to Astronautics*. New York: McGraw-Hill.

Vane, G., & Goetz, A. F. (1988). Terrestrial imaging spectroscopy. *Remote Sensing of Environment*, *24*(1), 1–29.

Weng, Q., & Quattrochi, D. A. (2007). *Urban remote sensing*. Boca Raton: CRC Press.

Zhang, J., Rivard, B., Sánchez-Azofeifa, A., & Castro-Esau, K. (2006). Intra-and inter-class spectral variability of tropical tree species at La Selva, Costa Rica: Implications for species identification using HYDICE imagery. *Remote Sensing of Environment*, *105*(2), 129–141.

Zhang, C., & Qiu, F. (2012). Mapping Individual Tree Species in an Urban Forest Using Airborne Lidar Data and Hyperspectral Imagery: *Photogrammetric Engineering and Remote Sensing*, *78*(10), 1079–1087.

THIS PAGE INTENTIONALLY LEFT BLANK

INITIAL DISTRIBUTION LIST

1. Defense Technical Information Center
   Ft. Belvoir, Virginia

2. Dudley Knox Library
   Naval Postgraduate School
   Monterey, California

3. Fred A. Kruse
   Naval Postgraduate School
   Monterey, California

4. Richard C. Olsen
   Naval Postgraduate School
   Monterey, California

5. Dan C. Boger
   Naval Postgraduate School
   Monterey, California